Research Article
DILI, Autoimmune, Cholestatic and Genetic Diseases

JOURNAL OF HEPATOLOGY

Integrative omics and phase IIa clinical trial identify TNF as key node in autoimmune hepatitis

Authors

Yang Xu, Jan Philipp Weltzsch, Christoph Kilian, …, Christoph Schramm, Nicola Gagliani, Ansgar Wilhelm Lohse

Correspondence

n.gagliani@uke.de (N. Gagliani), a.lohse@uke.de (A.W. Lohse).

Graphical abstract

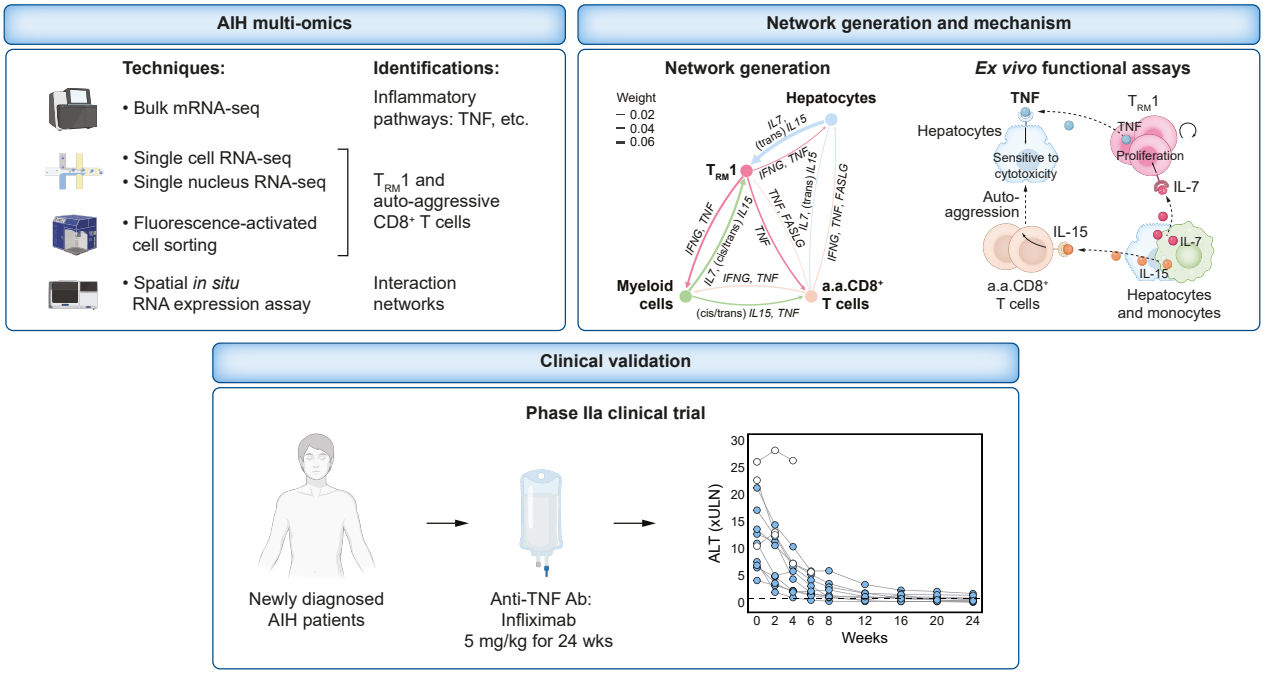

Highlights

- Type I cytokines, including TNF and downstream pro-inflammatory signaling, are central to the hepatic immune response in AIH.
- AIH pathology is sustained by a specific network of tissue-resident $CD4^+$ and $CD8^+$ memory T cells, myeloid cells, and hepatocytes.
- TNF acts as one of the cytokines linking the cellular nodes of this network.
- IL15-induced cytotoxic auto-aggression by $CD8^+$ T cells can kill hepatocytes, which is enhanced by $CD4^+$ T cell-derived TNF.
- Anti-TNF treatment demonstrates efficacy as an alternative to steroid-based induction therapy.

Impact and implications

These findings have significant implications for the treatment of autoimmune hepatitis (AIH). By mapping the spatial and functional immune network within the AIH liver, this study identifies IL-15 and TNF as central drivers of T cell-mediated cytotoxicity, offering new precision targets for intervention. The successful use of infliximab as a steroid-free therapy in a phase II trial marks a pivotal step toward safer, more specific treatment options for patients with AIH. This research not only advances our understanding of AIH pathogenesis, but also sets the stage for broader application of immune-targeted therapies in autoimmune liver diseases.

https://doi.org/10.1016/j.jhep.2026.02.026
 J. Hepatol. 2026, 85, 71–90

Research Article
DILI, Autoimmune, Cholestatic and Genetic Diseases

JOURNAL OF HEPATOLOGY

Integrative omics and phase IIa clinical trial identify TNF as key node in autoimmune hepatitis

Yang Xu[1,3,†], **Jan Philipp Weltzsch**[1,2,†], **Christoph Kilian**[1,2,4,†], Babett Steglich[1,2,3], Christina Weiler-Normann[2], Michael Dudek[5], Jonas Fackler[5], Malte H. Wehmeyer[2], Joseph Tintelnot[1,3,6], Laura A. Liebig[2,7], Silja Steinmann[1,2], Alena Laschtowitz[2], Ludwig J. Horst[2], Ida Schregel[2], Marcial Sebode[1,2], Johannes Hartl[2], Christian Casar[1,2], Jing Lu[1,3], Gerhard Schön[8], Antonia Zapf[8], Maria Rosa Bono[9], Mariana V. Rosemblatt[10], Sarah Nuñez[11], Justine Castañeda[12], Sören Alexander Weidemann[13], Nico Kaiser[14,15], Maria Schwerk[15], Manuela Kolster[1,16], Guido Rattay[1,3,16], Hanna Ulrich[1,2,4], Varshi Sivayoganathan[1,15], Ning Song[1,15], Jenny Krause[1,2,3], Marius Böttcher[1,2], Adrian Sagebiel[1,3,17], Jonas Wagner[1,3,17], Christian F. Krebs[1,15], Victor G. Puelles[15,18,19], Norbert Hübner[7], Eva Tolosa[1,16], Stefan Bonn[1,14,20], Samuel Huber[1,2], Percy A. Knolle[5], Johannes Herkel[1,2,‡], Lorenz Adlung[1,2,4,‡], Christoph Schramm[1,2,21,‡], Nicola Gagliani[1,3,*,‡], Ansgar Wilhelm Lohse[1,2,*,‡]

Journal of Hepatology **2026**. vol. 85 | 71–90

Check for updates

See Editorial, pages 18–20

Background & Aims: Patients with autoimmune hepatitis (AIH) experience increased mortality and severe side effects from non-specific immunosuppressive therapy, highlighting an urgent need for targeted treatment approaches. Here, we aimed to delineate the cellular and molecular network underlying AIH within its spatial context and to validate a key therapeutic target in a clinical trial.

Methods: We employed computational modelling, multi-omics analyses, and functional experiments to map the immune landscape of AIH. In addition, we conducted a steroid-free open-label phase IIa clinical trial using infliximab, a TNF-targeting antibody, in patients with AIH.

Results: Our studies revealed that myeloid cell and hepatocyte-derived IL-15 promotes cytotoxicity and proliferation of liver auto-aggressive $CD8^+$ T cells. Full execution of their cytotoxic program is licensed by TNF derived from clonally expanded liver-resident $CD4^+$ T cells. AIH hepatocytes respond to TNF by increasing expression of adhesion molecules, making them targets for both $CD8^+$ and $CD4^+$ T cells. In the clinical trial, targeting TNF with infliximab demonstrated efficacy as an entirely steroid-free AIH treatment.

Conclusions: These findings elucidate the immune network in AIH and identify TNF as one of the central network nodes. Accordingly, our findings provide the basis for novel targeted, steroid-free immune therapies, including the use of infliximab.

Clinical trial number: European Union Clinical Trials Register (EudraCT No.: 2017-003311-19).

Introduction

Autoimmune hepatitis (AIH) is a chronic inflammatory liver disease that can affect all age groups, including young children. AIH is associated with increased mortality in addition to increased morbidity.[1,2] A key histological feature of AIH is lymphocytic infiltrates, extending from the portal fields into the parenchyma of the liver (interface hepatitis).[3] If left untreated, the disease may lead to acute hepatic failure and, in less acute cases, may rapidly progress to liver fibrosis, cirrhosis, and hepatic decompensation with life-threatening complications or the need for liver transplantation. Non-specific immunosuppression with corticosteroids is the standard treatment for AIH, initially given at high doses as induction therapy, followed by lower doses in combination with maintenance therapies like azathioprine or mycophenolate mofetil. One of the most urgent clinical problems is that these pleiotropic drugs have significant side effects. Most patients strongly disfavor corticosteroid treatment as they experience a drastic and lasting reduction in quality of life due to the frequent occurrence of weight gain, metabolic bone disease, diabetes or depression.[4–6] Indeed, corticosteroid treatment is a major risk factor for major depression (five-fold) or osteoporosis (six-fold) in AIH, compared to the general population.[7,8] Despite the well-known adverse effects of steroids,

* Corresponding authors. Address: University Medical Center Hamburg-Eppendorf, Martinistraße 52, 20246 Hamburg, Germany; Tel.: +49 7410 52545.
E-mail addresses: n.gagliani@uke.de (N. Gagliani), a.lohse@uke.de (A.W. Lohse).
† These authors contributed equally to this work.
‡ These authors jointly supervised this work.
https://doi.org/10.1016/j.jhep.2026.02.026

recent registry data from six international centers revealed that only 27% of patients attain steroid-free remission after 1 year of treatment. Accordingly, most patients require long-term corticosteroid treatment to achieve this therapeutic goal.[9] The frequent occurrence of adverse effects may thus explain why more than 55% of patients with AIH worry about their corticosteroid therapy most or all of the time.[6] Therefore, targeted, preferably steroid-free therapeutic approaches for AIH combining efficacy with better tolerability are urgently needed.[10]

The development of targeted treatments for AIH is currently impeded by the lack of a concept that coherently and comprehensively integrates the various components of the liver immune landscape in AIH. AIH is associated with increased activation and numbers of cells of both the innate and adaptive immune response. Accumulation and activation of monocyte-derived macrophages correlate with disease severity.[11–13] The importance of the adaptive immune response, in particular of $CD4^+$ T cells, is indicated by a strong genetic linkage to the HLA-DRB1*0301 and HLA-DRB1*0401 haplotypes.[3,14] In keeping with this, AIH is characterized by increased hepatic infiltration and expansion of $CD4^+$ T cells.[3] While self-reactive $CD4^+$ T cells have been detected in the peripheral blood of patients with AIH,[15–17] the role of $CD4^+$ tissue-resident memory T (T_{RM}) cells — identified in healthy livers as $CD4^+$ $CD69^+$ $CD49a^+$ T cells — has only recently begun to be described in AIH.[18] We have previously shown that liver $CD4^+$ T cells can co-produce IFN-γ and TNF in AIH.[19] This analysis was restricted to only a few markers, therefore a systematic and unsupervised characterization of liver $CD4^+$ T cells, their cellular network and their function in AIH remains to be performed.

Recently it has been shown that the number of liver-resident $CD8^+$ T_{RM} cells, identified as $CD8^+$ $CD69^+$ $CD103^+$ T cells displaying a cytotoxic profile, correlates with the severity of AIH.[20] These cells seem to express CD69 and CD103 in response to IL-15.[20] This cytokine has been shown to promote an auto-aggressive (a.a.) function in mouse and human liver $CD8^+$ T cells in metabolic dysfunction-associated steatohepatitis (MASH).[21] In the context of MASH, $CD8^+$ T cells assuming an a.a. state, from here on defined as a.a.$CD8^+$ T cells, can promote hepatocyte damage.[21] The presence and potential role of a.a.$CD8^+$ T cells in patients with AIH remain unknown.

In addition, the mechanisms by which innate and adaptive immune cells collectively establish a network that culminates in uncontrolled liver damage and lymphocyte accumulation – the hallmark histopathological feature of AIH – remain unclear.

Here we combine multi-omics and functional experiments to explore the topology of the immune network in AIH and identify its key nodes. We uncover critical cytokines and signaling pathways correlated with the grade of liver inflammation (*e.g. TNF*, *IFNG*) and delineate the respective contributions and spatial localization of different immune cell types (*e.g.* a.a.$CD8^+$ T cells) and hepatocytes that together cause liver damage in AIH. In parallel, one of the identified cytokines, TNF, was targeted in a phase IIa clinical trial using the anti-TNF antibody infliximab, demonstrating the efficacy of anti-TNF therapy in patients with newly diagnosed active AIH and highlighting an opportunity for steroid-free treatment of patients with AIH. These findings confirm the validity of our integrative omics approach and provide a resource for the identification of additional therapeutic targets in AIH, which might also be used as a blueprint for other autoimmune diseases.

Materials and methods

Patient populations and liver samples

For bulk mRNA-sequencing analysis, we included liver biopsies from 16 patients with AIH and 11 patients with primary biliary cholangitis (PBC);[22] samples were stored in liquid nitrogen and sequenced together. For cellular indexing of transcriptomes and epitopes by sequencing (CITE-seq) analysis, we included liver biopsies and paired blood samples from 10 patients with active AIH (eight of the patients were untreated, one received prednisolone for only a few days prior to biopsy, one relapsed on a low dose of budesonide); samples were processed while fresh. For single-nucleus RNA sequencing (snRNA-seq) analysis, we included liver biopsies from six patients with AIH (five of the patients were untreated and distinct from the CITE-seq atlas donors, while one patient was included in the CITE-seq and had been started on emergency prednisolone for a few days as mentioned above); samples were stored in liquid nitrogen and sequenced together. For flow cytometry and *in vitro* functional studies (FACS dataset), we included liver biopsies and paired blood samples from 13 patients with AIH and six controls who underwent bariatric surgery, benign liver lump resection, breast cancer liver metastasis resection, or liver biopsy with unremarkable pathological findings; samples were processed while fresh. For Xenium spatial *in situ* RNA expression assay, formalin-fixed paraffin-embedded liver biopsies from six patients with AIH and three controls (unremarkable pathological findings) were used. The bulk mRNA sequencing, AIH atlas (CITE-seq and snRNA-seq), FACS, and Xenium spatial *in situ* RNA expression assay datasets each represent an independent cohort of patients with AIH.

All samples were collected at the University Medical Centre Hamburg-Eppendorf, and the studies were approved by the Ethics commission Hamburg (Ethikkommission der Ärztekammer Hamburg, Germany). Biopsies were obtained via minilaparoscopy using a TruCut needle, a standard procedure at our center. AIH diagnosis was established according to current guidelines and the 'Simplified Criteria for the Diagnosis of AIH'.[3,23] Histological and laboratory parameters were collected alongside tissue samples for all the patients. For clinical characteristics, see Table S4–7.

Multi-omics workflow

The multi-omics workflow, including bulk mRNA sequencing, CITE-seq and snRNA-seq, and Xenium spatial *in situ* RNA expression assay, together with their associated bioinformatic analyses (data pre-processing, integration, dimensionality reduction, clustering, and interactome analysis) and sample preparation, is described in the supplementary methods.

Flow cytometry

Antibodies for flow cytometry are listed in Table S1 (CTAT table). For surface protein staining without cell stimulation, human liver and blood single cell suspensions were first stained with Zombie UV Fixable Viability Kit (BioLegend) on ice for 10 min. In a second step, the single cell suspension was stained with antibodies in PBS containing 1% FCS (PAN Biotech) and 2 mM EDTA on ice for 1 h. For the detection of TNF and IFN-γ, cells were thoroughly washed after surface

staining and subsequently stimulated with 50 ng/ml PMA, 1 μmol/L Ionomycin (both from Sigma-Aldrich) in the presence of Brefeldin-A solution (1:1,000, BioLegend) in RPMI medium (Gibco) with 10% FCS for 2 h at 37 °C. Dead cells were further labeled using the Zombie UV Fixable Viability Kit following the protocol as described above. Subsequently, cells were fixed and permeabilized using the Fixation/Permeabilization Kit (BD Biosciences) according to the manufacturer's instructions, then stained intracellularly with fluorochrome-labeled antibodies against IFN-γ and TNF. For the detection of granzymes, following cell viability and surface staining, cells were fixed and permeabilized as described above without stimulation. Intracellular staining was then performed using fluorochrome-labelled antibodies against granzyme A, B and K. Flow cytometric analysis was conducted using a FACS LSR Fortessa A3 (BD Bioscience), and FACS cell sorting was conducted using a FACS AriaFusion (BD Bioscience). Data analysis was performed using the FlowJo software (v10.4).

Cell culture

Ex vivo *expansion of primary human T cells*
Primary $T_{RM}1$ and a.a.$CD8^+$ T cells from AIH livers, $CD4^+$ and $CD8^+$ T_{EM} cells from paired AIH blood, as well as blood regulatory T cells from healthy donors were FACS sorted. The sorted cells were immediately cultured for *ex vivo* expansion in X–VIVO medium (Lonza) by stimulation with 2.5 μg/ml PHA (Sigma-Aldrich) and 40 Gy-irradiated peripheral blood mononuclear feeder cells in the presence of recombinant human IL-2 (Miltenyi), 50 U/ml for $CD4^+$ T cells and 100 U/ml for $CD8^+$ T cells, respectively. On day 12, the expanded cells were either cryopreserved or subjected to a second round of expansion.[24]

Induction of a.a.$CD8^+$ T cells in vitro
$CD8^+$ T cells were isolated from the blood of healthy, voluntary donors after they gave written and informed consent. This study was approved by a vote from the ethics committee of the University Hospital München rechts der Isar (564/18S). Blood was mixed 1:1 with PBS and loaded on Pancoll (PAN Biotech), followed by centrifugation at 1,400 g for 25 min to isolate peripheral blood mononuclear cells. Cells were washed, counted and subjected to immunomagnetic separation for $CD8^+$ T cells using human CD8 MicroBeads (Miltenyi Biotec), according to the manufacturer's protocols. To induce a.a.$CD8^+$ T cells, purified $CD8^+$ T cells were stimulated with 10 ng/ml IL-15 (PeproTech) for 2 days prior to the analysis.

Impedance-based K562 cytotoxicity assay
The dynamics of T-cell cytotoxicity against the HLA-deficient cell line K562 (myelogenous leukemia) over time were measured using impedance-based technology on an xCELLigence RTCA MP device (ACEA Biosciences). In brief, cells of the non-adherent cell line K562 were attached to the bottom of a plate (10^4 cells/well) using anti-CD71 (BioLegend) antibodies that were coated on the plate 18 h before. After 48 h (K562 cells reached confluency and maximum cell index), 10^5 $T_{RM}1$ and a.a.$CD8^+$ T cells from the liver, and 10^5 paired blood-derived effector memory $CD4^+$ and $CD8^+$ T cells from the same patients with AIH were added to the wells. Measured electrical impedance is shown as cell index and normalized to the time point the co-culture of T cells with target cells was started. The cell index was measured 24 h after co-culture was started to evaluate the efficacy of target cell killing. The percentage of killing was calculated by subtracting the cell index values from controls (target cells alone).

Impedance-based primary hepatocyte cytotoxicity assay
Primary human hepatocytes were purchased from PELOBiotech and Lonza. After thawing, cell viability was determined by Trypan blue dye exclusion. 40,000 hepatocytes were seeded and cultivated on plates coated with rat tail collagen R (Advanced Biomatrix) in Williams E medium containing insulin-transferrin-selenium, 1.5% bovine serum albumin, GlutaMAX, non-essential amino acids, 100 U/ml penicillin-streptomycin (all supplements from Gibco) in the presence of 10% FCS for 16 h. Hepatocytes were maintained in medium lacking FCS for 2 days before being subjected to experiments. 100 μl supernatants from $T_{RM}1$ cells from AIH livers activated by anti-CD3/anti-CD28 beads (Gibco) were added to hepatocyte cultures for 24 h. In some conditions, 10 μg/ml anti-TNF neutralizing antibody (BioXcell) was added concurrently. Following this pre-treatment, the medium was replaced, and 10^5 autologous or HLA-A-matched blood $CD8^+$ T cells pre-exposed to IL-15 were added to the hepatocytes. Cell viability was then monitored for an additional 15 h using impedance-based technology by xCELLigence as described above.

Flow cytometry-based K562 cytotoxicity assay
Cytotoxicity measurement was performed by labelling target cells with CFSE (ThermoFisher) and incubating with effector cells in different effector-to-target ratios for 24 h. In some conditions, K562 cells were treated with 50 ng/ml recombinant human TNF (Peprotech) or with supernatant of $T_{RM}1$ cells from AIH livers activated with anti-CD3/anti-CD28 beads in the presence of 10 μg/ml anti-TNF neutralizing antibody (BioXcell) for 24 h before co-culture with a.a.CD8+ T cells. Dead K562 cells in co-culture with $CD8^+$ T cells were detected by flow cytometry.

Stimulation of $T_{RM}1$ and a.a.$CD8^+$ T cells in vitro
To assess IL-7 or IL-15 induced proliferation *in vitro*, expanded $T_{RM}1$ and a.a.$CD8^+$ T cells from the liver of AIH patients were rested and labelled with CellTrace Violet (Thermo Fisher) according to the manufacturer's protocol. Cells were cultured in X–VIVO medium (LONZA) supplemented with recombinant human IL-15 or IL-7 (both from R&D Systems) at concentrations specified in the figures. Cells were harvested on the indicated days. Their expansion was quantified by measuring CellTrace Violet dye dilution using flow cytometry.

To evaluate the cytokine profile of $T_{RM}1$ cells at protein level after *ex vivo* expansion, expanded cells were cultured in X–VIVO medium and stimulated with the ImmunoCult Human CD3/CD28 T Cell Activator (STEMCELL Technologies) according to the manufacturer's protocol. Supernatants were collected on the specified days, and cytokine levels were quantified by flow cytometry using the LEGENDplex Human CD8/NK Panel (BioLegend), following the manufacturer's instructions.

Detection of STAT5 phosphorylation

Frozen $T_{RM}1$ and a.a.$CD8^+$ T cells from the liver of AIH patients were thawed, rested in RPMI at 4 °C for 1 h, and stained with

fluorochrome-labelled CD4 and CD8 antibodies (BioLegend), and viability dye AF750 NHS Ester (Thermo Fisher). Cells were stimulated with 10 ng/ml recombinant human IL-15 (R&D Systems or PeproTech as specified) or 100 U/ml recombinant human IL-2 (Miltenyi) in RPMI at 37 °C for 15 min, fixed with 2% PFA at 37 °C for 15 min, permeabilized with 100% methanol on ice for 30 min, and stained with pSTAT5 antibody (Thermo Fisher) for 1 h at room temperature. The readouts were acquired by flow cytometry.

Clinical trial (AIH-MAB)

In this phase IIa, proof-of-concept clinical trial, we evaluated the effect of intravenous infliximab as the first corticosteroid-free induction treatment for patients with acute and previously untreated AIH. The trial protocol was approved by the local ethics committee (Ethikkommission der Ärztekammer Hamburg, Approval No. PVN5646-3952) and registered within the European Union Clinical Trials Register (EudraCT No.: 2017-003311-19). The study was conducted in accordance with the Declaration of Helsinki.

Patients

Between October 2018 and February 2023, 13 patients were screened for enrolment in the clinical trial, of whom 12 were consecutively enrolled. Patients aged 18-65 years who were considered to have possible or probable AIH, and who exhibited a treatment requirement as defined by current guidelines (modified hepatic activity index [mHAI] ≥4/18), were eligible for inclusion in the trial. Patients with concomitant liver disease besides AIH, history of decompensation of cirrhosis or liver failure were excluded from participation in the trial. Detailed information on inclusion/exclusion criteria is provided in the trial protocol (supplementary material). The study results were additionally compared to data from 24 patients included from Hamburg to the prospective R-LIVER registry,[9] who received the current standard of care (SoC) with corticosteroids (prednisolone or budesonide) and azathioprine (or 6-mercaptopurine/mycophenolate in case of intolerance), using propensity score matching (PSM; see "Statistical Analyses" in the supplementary material). All participating patients provided written informed consent before enrolment.

Experimental treatment

Patients in the trial received a cumulative total of 8 doses of intravenous infliximab (Inflectra®, Pfizer) at a dosage of 5 mg/kg over a period of 24 weeks (day 0, weeks 2, 6, 8, 12, 16, 20, and 24). In addition, patients were followed up during additional safety visits in weeks 1 and 4 and were monitored after completion of the infusion therapy at weeks 36 and 48. All patients additionally commenced azathioprine therapy after the week 2 visit at an initial dose of 50 mg daily, which was subsequently titrated in 25-50 mg increments every 7 days to achieve a target dose of 1-2 mg/kg body weight per day. In case of intolerance, patients were switched to 6-mercaptopurine (50 mg/day) or mycophenolate (2,000 mg/day).

Safety and monitoring

Patients were screened twice within 2 weeks prior to treatment initiation. Physical examinations, as well as assessments of vital signs and body weight, were performed at every visit as were standard laboratory values. Visits included a safety evaluation regarding clinical and biochemical safety endpoints or (serious) adverse events (AEs). Serious AEs, including their severity and likelihood of a causal relationship to infliximab administration, were documented, followed up, and reported within 24 h, where applicable. Liver stiffness was assessed by transient elastography (Fibroscan®) during screening as well at week 12, 24, 36 and 48. Quality of life was assessed using standardized questionnaires (SF-36 [Short Form-36 Health Survey]) at the time of screening, initial administration, as well as at weeks 1, 4, 8, 12, 16, 20, 24, 36, and 48. Patients were withdrawn from infliximab treatment in the event of severe adverse events considered related to the study medication. Participation in the study was also discontinued in case transaminase levels increased more than 20% over the respective patient's individual baseline during the first 4 weeks of treatment or in those who exhibited a decrease of transaminase levels <50% 8 weeks after treatment initiation. In this case, patients received standard treatment with corticosteroids in accordance with current guidelines.

Endpoints

The primary endpoint of the study was defined as biochemical remission at month 6 after treatment initiation. Biochemical remission was specified as normalization of alanine aminotransferase (ALT) and aspartate aminotransferase (AST) (≤35 U/L for females and ≤50 U/L for males) as well as of IgG (≤16 g/L). Secondary endpoints were defined as differences in health-related quality of life (HRQoL) as assessed by the questionnaires mentioned above as well as decrease in liver stiffness (measured by transient elastography/FibroScan®) and the absence of weight gain (BMI).

Statistical analyses

Statistical analyses are described in the supplementary materials.

Results

Identification of inflammatory pathways associated with the severity of AIH

To characterize the signaling molecules, transcription factors and cytokines constituting the inflammatory process of AIH, and to identify potential drug targets, we profiled the bulk transcriptome of liver biopsies obtained from 16 patients with active AIH. As controls, we included biopsies from 11 patients with another autoimmune liver disease, namely PBC. Standard liver biochemistry and histological grading were used to evaluate disease activity and stage (Fig. 1A). ALT serum levels and the mHAI were assessed primarily, as they are regarded as the best markers of inflammatory activity in the clinical context of AIH. Considering these features, a principal component analysis showed that the transcriptomes of the liver samples were separated by mHAI rather than by diagnosis or by fibrosis stage (Fig. 1B, multivariate PERMANOVA $p_{mHAI} = 0.03$, $p_{diagnosis} = 0.25$, $p_{fibrosis} = 0.19$). Next, to further evaluate how the clinical markers represent inflammatory activity at the gene expression level, we used the MSigDB gene set "Hallmark Inflammatory Response" (M5932) to calculate a patient-wise inflammation score. As expected, patients with PBC

exhibited relatively low scores compared to AIH. Furthermore, we found that biopsies showing severe histologic activity (*i.e.* mHAI ≥10) showed a markedly increased expression of pro-inflammatory genes (Fig. 1C). In addition, there was a strong association between the inflammation score and serum ALT levels in patients with AIH, which was not observed in the PBC cohort (Fig. 1C). These results showed that the clinical signs of inflammation were reflected at the transcriptome level.

Next, we analyzed the expression of key cytokines. To this end, we determined the association between gene expression and clinical features in patients with AIH by applying spearman's rank correlation (r_s) (Fig. S1A). Subsequently, we performed a KEGG enrichment analysis on genes ranked by r_s. We found that in terms of signal transduction, the TNF-, NFKB- and JAK-STAT signaling pathways in particular were positively associated with histologic and laboratory features of inflammation (Fig. 1D). Consistently, when we inferred the transcription factor activity by applying a univariate linear model between the gene correlation and the gene regulatory network CollecTRI,[25] transcription factors annotated to the previously identified pathways (*e.g.* STAT1, RELA, NFKB1) were among the top hits (Fig. 1E).

In accordance with the identified pathways, several ligands (*e.g*. *TNF*, *IL12A*, *IFNG, IL15*) exhibited a strong correlation to both features of inflammation, mHAI and ALT (Fig. 1F and S1B). To validate our findings, we examined the expression of selected cytokine genes by real-time PCR in samples from the AIH and PBC cohorts (Fig. 1G). In line with the bulk mRNA-sequencing data, an association between mRNA levels and both mHAI and ALT was confirmed.

These analyses suggested that the type I cytokines TNF, IL-12, IFN-γ and the corresponding pro-inflammatory downstream signaling in the liver are central players in the inflammatory pathophysiology of AIH, and thus might be promising therapeutic targets. However, the specific cellular network encompassing these inflammatory pathways remained unclear.

Development of an AIH atlas integrating liver immune and non-immune cell transcriptomes

To reveal the cellular network related to the AIH-specific pro-inflammatory pathways identified above, we assembled a comprehensive single-cell RNA sequencing atlas of the immune and non-immune cells found in AIH livers, using a patient cohort distinct from the one shown in Fig. 1. To this end, we analyzed fresh liver biopsies from 10 patients with AIH. Moreover, to discriminate between systemic and tissue-specific immune mechanisms, we also analyzed paired peripheral blood samples collected from 3 of those patients taken at the same time as the respective fresh liver biopsies (Fig. 2a). $CD45^+$ immune cells from the liver biopsies and $CD3^+$ T cells from paired blood samples were FACS-sorted and subjected to CITE-seq and single-cell T-cell receptor sequencing (scTCR-seq). The capture of non-immune cells, particularly hepatocytes, was technically challenging. To overcome this, we isolated nuclei from cryopreserved liver biopsies of six patients with AIH (one of whom also contributed a sample to the CITE-seq/scTCR-seq dataset introduced above) and performed snRNA-seq (Fig. 2A).

To simultaneously depict the immune and non-immune profiles in the liver of patients with AIH and achieve robust clustering, we integrated our CITE-seq dataset with the snRNA-seq dataset. Cells recovered from fresh CITE-seq predominantly comprised immune cells, while cells recovered from cryopreserved snRNA-seq encompassed both immune and non-immune cell types (Fig. 2B). Although CITE-seq and snRNA-seq show different sequencing depths (Fig. S2A), by integrating the CITE-seq and snRNA-seq datasets, we identified similar populations to those derived from the analysis of the two datasets independently (Fig. S2B–D). This showed the validity of the integration approach used here.

Next, we annotated the identified major clusters from both immune and non-immune cells in the liver based on a combination of differentially expressed genes (DEGs) in a semi-supervised approach. Immune cell clusters encompassed $CD4^+$ T cells, $CD8^+$ T cells, B cells, plasma cells, innate-like T cells, and myeloid cells (including monocytes, macrophages and dendritic cells), while non-immune cells included hepatocytes, endothelial cells, cholangiocytes, and stellate cells/fibroblasts (Fig. 2c and S2E,F). Considering that the strong association of AIH with specific HLA-DR haplotypes suggests a T cell-driven immune response,[3,14] and the recent description of $CD8^+$ T_{RM} cells in AIH,[20] we further investigated liver-derived T cells. We annotated nine major $CD4^+$ T-cell clusters, including naïve-like T cells, central memory T cells (T_{CM}), five effector memory T-cell clusters (T_{EM}-a, -b, -c, -d, -e) and two $FOXP3^+$ regulatory T-cell clusters (T_{REG}-a, -b) (Fig. 2D and S3A,B). Following the same approach, we annotated 12 major $CD8^+$ T-cell clusters including a naïve-like cell cluster, two T_{CM} (T_{CM}-a, -b) and seven effector memory T-cell clusters (T_{EM}-a, -b, -c, -d, -e, -f, -g) (Fig. 2E and S3C,D).

Hepatocytes have distinct functions based on their location in the hepatic lobule, a concept known as zonation.[26] Zone 1 consists of periportal hepatocytes surrounding the portal triad, zone 2 comprises the mid hepatocytes, and zone 3 includes central hepatocytes located near the central vein. We annotated ten distinct hepatocyte clusters (Fig. 2F and S3E,F), three of which expressed gene signatures representing the three zonation populations, periportal, midzone, and central hepatocytes. Moreover, we found an inflammatory cluster with high expression of immune regulation-related genes, such as *IL32, ICAM1 and STAT1*, reflecting the involvement of hepatocytes in the inflammatory process in AIH. Additionally, two proliferative clusters and one *BICC1*-high cluster were annotated, which probably reflect disease-related damage and subsequent regenerative responses of hepatocytes.[27,28] We also annotated two clusters with unclear biological relevance as *PTPRB*-hi and *PTPRC*-hi, which co-express hepatocyte genes with endothelial (*PTPRB*) or immune cell-related (*PTPRC*) genes, respectively. Their functional relevance requires further investigation.

In conclusion, we generated a comprehensive single-cell AIH atlas which enables the study of immune and non-immune cells and their potential interactions in the liver.

Identification of $CD4^+$ $T_{RM}1$ cells in AIH liver

Based on the DEGs and signature genes, we refined the annotation of the liver $CD4^+$ T_{EM} clusters and within them identified T_{FH} cells (former T_{EM}-d) and T_R1 cells (former T_{EM}-e). In our effort to identify clusters relevant to AIH, we found that

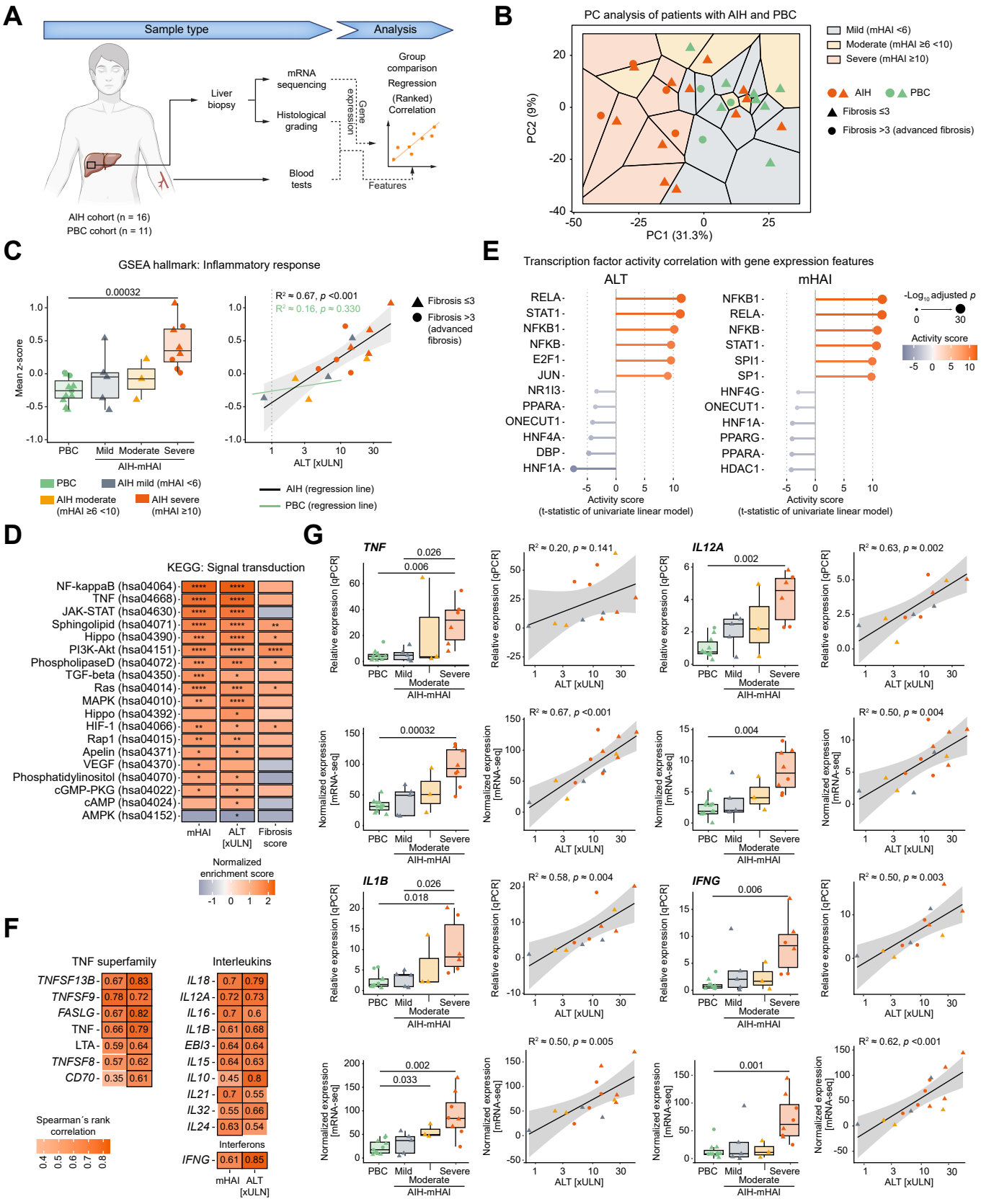

Fig. 1. AIH disease activity is correlated with pro-inflammatory pathways and cytokines identified by bulk mRNA sequencing. (A) Overview of the sampling and analysis pipeline. (B) Principal component analysis of patients with AIH and PBC based on the 500 most variable genes. Point shapes distinguish advanced fibrosis, while point colors depict the diagnosis. The colors of the Voronoi fields represent disease activity as measured by mHAI. (C) Inflammation score based on the MSigDB hallmark gene set "Inflammatory Response". Left: Boxplot showing inflammation scores by diagnosis. Patients with AIH were further stratified by mHAI.

the cluster T_{EM}-c was enriched for *TNF* and *IFNG*, two of the cytokines which we found to be associated with AIH and correlated with disease states, as shown above (Fig. 1). Accordingly, this cluster was also enriched for the type 1 master transcription factor *TBX21* and molecules associated with cytotoxicity, such as *TNFSF10 and FASLG* (Fig. 3A). In addition, although not the only one, this cluster was clonally expanded (Fig. 3B and S4A). Using the TCR sequences (Fig. S4B and C), we found that 80% (8 out of 10) of the most highly expanded clonotypes (n ≥6 clones) within the T_{EM}-c cluster were present in the liver, but not in the blood (Fig. 3C). In contrast, clonotypes that were expanded at lower levels (n ≤5 clones) could be detected both in the liver and in the blood of the same patients (Fig. S4D). As these findings suggested a possible residency of the highly expanded clones within the T_{EM}-c cluster, we tested for the expression of a literature-based residency and migratory score[29] and observed that the T_{EM}-c cluster was enriched for genes associated with residency but not with migration, particularly in comparison with T_{EM}-a cells, which were *S1PR1*-positive, thus favoring egress from the tissue (Fig. 3D). Considering the type 1 cytokine profile, residency signature and in particular the expression of two widely accepted prototypical residency markers, *CD69* and *CXCR6* (Fig. S4E), we propose referring to T_{EM}-c as tissue resident-like type 1 memory (T_{RM}1) cells.

To confirm the presence and the features of T_{RM}1 cells, we validated the AIH atlas findings at the protein level using multiparametric flow cytometry on a new set of AIH tissue samples. We first selected potential T_{RM}1 surface markers from the CITE-seq data accepted in the field, *i.e. CD69*, *CXCR6*, *ITGA1* and *TIGIT* (Fig. S4E). *CD69* and *CXCR6* were expressed in T_{RM}1 cells but not in migratory T_{EM}-a cells. *ITGA1*, which is commonly used to identify type I cytokine-producing and resident cells,[30] appeared to be expressed, albeit by few cells, mainly in the T_{RM}1 cluster. Finally, *TIGIT* was selectively expressed in T_{FH} and regulatory cells,[31] as expected, but not in T_{RM}1 cells. Once these markers were selected, we tested them on cells isolated from fresh liver biopsies of patients with AIH. We hereby identified a distinct population of memory $CD4^+$ T cells co-expressing CD69, CXCR6, CD49a (encoded by the *ITGA1* gene) but negative for TIGIT, and thus probably reflecting T_{RM}1 cells (Fig. 3E and S4F). Considering that one of the key features of T_{RM}1 cells is the expression of *TNF* and *IFNG*, we restimulated liver $CD4^+$ T cells *in vitro* and found that the majority of the $CD69^+$ $CD49a^+$ $CD45RO^+$ $CD4^+$ T cells co-produced TNF and IFN-γ (Fig. 3F left, and S4G). Using a complementary analysis, we found that the majority of TNF and IFN-γ co-producing $CD4^+$ T cells were $CD69^+$ $CD49a^+$ $CD45RO^+$ $CD4^+$ T cells (Fig. S4H). Finally, we found that T_{RM}1 cells showed the highest average expression of both TNF and IFN-γ, as indicated by mean fluorescence intensity, followed by $CD69^-$ cells in the liver-infiltrate and blood T_{EM} cells (Fig. 3F, middle and right). Further confirmation of the phenotype of T_{RM}1 cells in the liver of patients with AIH was obtained by the capacity of $CD69^+$ $CD49a^+$ $CD45RO^+$ $CD62L^-$ $CD4^+$ T cells to produce granzyme A, B, and K, as was also indicated in the AIH atlas dataset (Fig. S4I). Finally, we tested whether T_{RM}1 cells were more abundant in AIH livers compared to mildly inflamed livers in various other conditions. We found a higher abundance of T_{RM}1 cells per milligram of liver in patients with AIH compared to controls (Fig. S4J).

Identification of a.a.$CD8^+$ T cells in AIH liver

Following a similar approach to that used for $CD4^+$ T cells, we also characterized liver $CD8^+$ T cells. In the livers of patients with MASH, Dudek *et al.* reported a population of a.a.$CD8^+$ T cells expressing the chemokine receptor CXCR6, along with key cytokines, including TNF and IFN-γ,[21] which we also observed in AIH livers a.a.$CD8^+$ T cells represent a state of $CD8^+$ T cells characterized by transient MHC I-independent cytotoxic capacity under conditions of IL-15 exposure.[21] We therefore wondered whether $CD8^+$ T cells, present in AIH livers, were characterized by the a.a. state. To address this, we first analyzed *CXCR6* and *CD69* expression in our sequencing data (Fig. S5A). Although *CXCR6* was expressed by fewer cells within the T_{EM}-a cluster, it was broadly expressed at the RNA level across T_{EM}-b to -g. Similarly, the tissue residence marker CD69 was widely expressed at the protein level from T_{EM}-a to -g. We further assessed the presence of an a.a. gene signature, assigning a.a. scores to each cluster.[21] We found that $CD8^+$ T_{EM}-a to -g exhibited elevated a.a. scores compared to the other clusters, namely naïve-like and T_{CM} cell clusters (Fig. 3G and S5B). Consistent with the a.a. potential, T_{EM}-f and -g were enriched for AIH-associated pro-inflammatory genes, such as *TNF* and *IFNG* (Fig. S5A). In addition, T_{EM}-d and -e were enriched for cytotoxicity-related genes, such as *FASLG*, *PRF1* and *GZMB* (Fig. S5A). All $CD8^+$ T-cell clusters except for the naïve-like cluster exhibited large clonal expansion (Fig. 3H and S5C). By analyzing TCR sequences from the three paired blood and liver samples, we identified 16 highly expanded clonotypes (n ≥31 clones). Notably, 50% (8 out of 16) of these clonotypes were exclusively present in the liver but not in the blood, and were found within T_{EM}-e, -g, as well as partially within T_{EM}-c, -d and -f. In contrast, the other 50% of highly expanded clonotypes were detectable both in the liver and blood and were primarily associated with clusters T_{EM}-a, -b, -c and partially T_{EM}-d and -f (Fig. 3I). Clonotypes with lower expansion (n ≤30 clones) exhibited a similar pattern (Fig. S5D). Collectively, these findings suggest longer dwell times of the cells of the T_{EM}-e and T_{EM}-g clusters in the liver, whereas the cells of the T_{EM}-a cluster appear more circulatory. Meanwhile, the T_{EM}-b, -c, -d and -f clusters might represent an

Significant differences are indicated by Wilcoxon Rank Sum test, FDR adjusted. Right: Linear regression plot for patients with AIH (black regression line, black dots) and PBC (green regression line; dots omitted). (D) Enrichment of KEGG terms in the "signal transduction" category for genes using the Spearman correlation to mHAI, ALT, or fibrosis scores in patients with AIH. Only terms significant for at least one feature are shown. Statistical significance is indicated as follows: *p <0.05, **p <0.01, ***p <0.001 and ****p <0.0001. (E) Bar plots of the top six transcription factors per feature with the highest activity scores, calculated using the t-statistic of a univariate linear model on the CollecTRI Database and strongly correlating genes. (F) Heatmap of strongly correlating tumor necrosis factor superfamily members, interleukins and interferon. r_s values are labelled. Fields with r_s >0.6 are emphasized by black border. (G) Boxplots and regression plots comparing normalized expression by mRNA sequencing with relative expression by qPCR for selected cytokines. AIH, autoimmune hepatitis; ALT, alanine aminotransferase; FDR, false discovery rate; mHAI, modified hepatic activity index; PBC, primary biliary cholangitis.

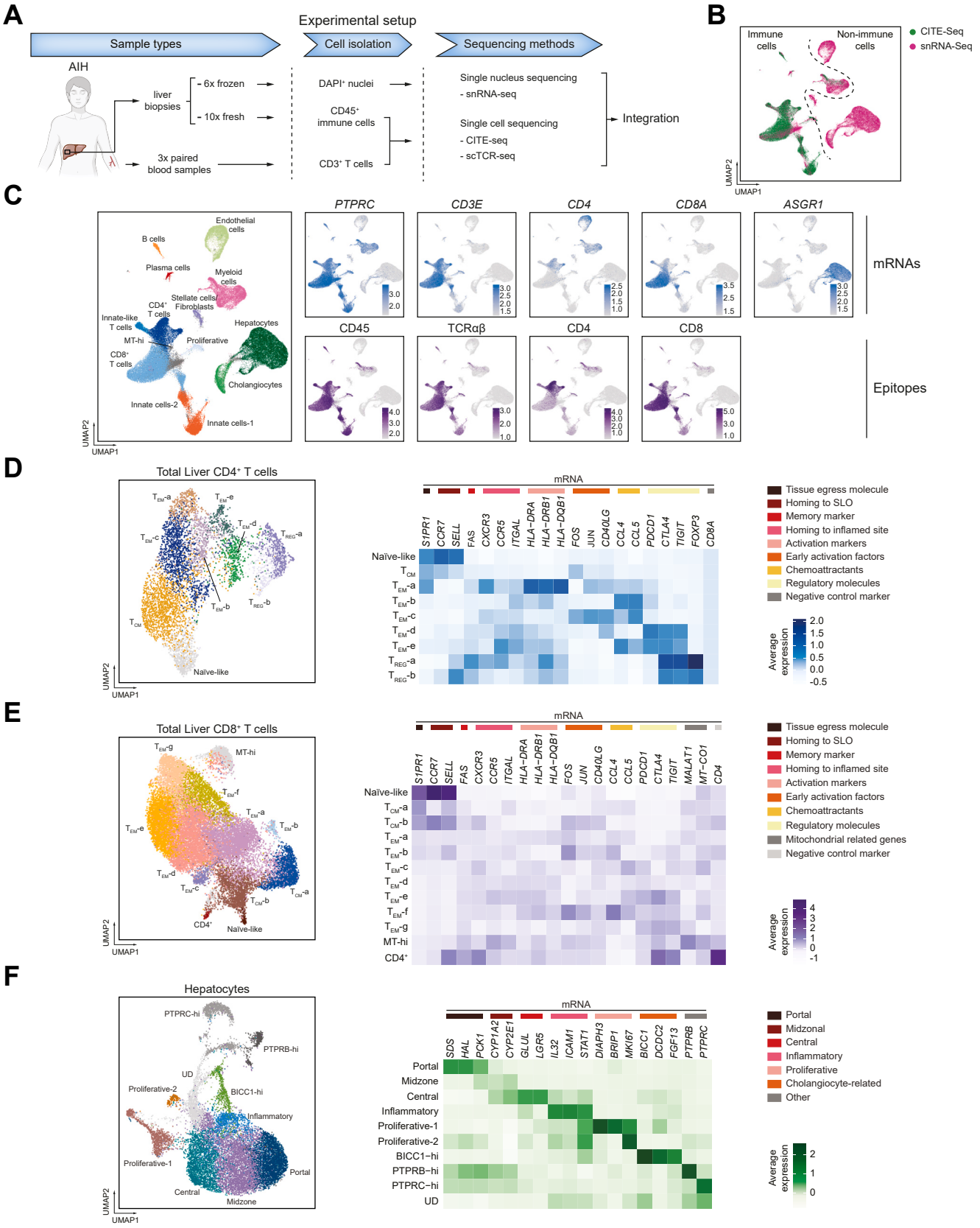

Fig. 2. Single-cell atlas of AIH liver. (A) Schematic representation of the experimental workflow using a patient cohort distinct from that in Fig. 1 (CITE-seq n = 10; snRNA-seq n = 6; with only one overlapping donor between the two sequencing datasets). (B) UMAP of all cells and nuclei from AIH livers colored by data source, reveals distinct clustering patterns that separate immune cells from non-immune cells. (C) Left: UMAP of 74,102 cells/nuclei (CITE-seq: n = 31,876; snRNA-seq: n = 42,226), color-coded by cell types. Right: Expression of key marker genes and epitopes. (D) Left: Sub-clustering analysis of CD4+ T cells, including 14 patients (2

intermediate state, consisting of some cells with a residency path and others adopting a circulatory pattern. Using residency and migratory scores as described above, T_{EM}-e, -f, and -g exhibited a higher residency score and a lower migratory score, albeit with some heterogeneity, compared to the other clusters. T_{EM}-a to -d exhibited an intermediate residency score (Fig. 3J). In short, these $CD8^+$ T_{EM} subclusters consist of cells with a potential migratory progression, transitioning from infiltrating to resident or vice versa. Nevertheless, based on the similar expression of the a.a. score, suggesting a potential common cytotoxicity function and the expression of the key markers CD69 and CXCR6, we simplified the potential heterogeneity of the T_{EM}-a to -g cell clusters by referring to them as $CD8^+$ T cells with a potential a.a. function (*i.e*. a.a.$CD8^+$ T cells).

As for $CD4^+$ $T_{RM}1$ cells, we confirmed the presence and characteristics of a.a.$CD8^+$ T cells at the protein level using multiparameter flow cytometry. We identified a distinct population co-expressing CD69 and CXCR6, which have been used to identify a.a. T cells (Fig. 3K and S4F). Additionally, this population also co-expressed PD-1 and TIGIT, which are additional surface markers identified in the a.a. gene set, reflecting their status as highly activated cells.[32] In contrast, the CXCR6 and CD69 double-negative population exhibited relatively low expression of PD-1 and TIGIT. Notably, CD49a, although not yet associated with auto-aggression, was also expressed by $CD69^+$ $CXCR6^+$ a.a.$CD8^+$ T cells (Fig. 3K). Upon *in vitro* restimulation, a large fraction of liver $CD69^+$ $CD49a^+$ $CD45RO^+$ $CD8^+$ T cells co-produced TNF and IFN-γ, further lending support to the notion that these cells represent a.a.$CD8^+$ T cells in accordance with our CITE-seq analysis (Fig. 3I and S5E). Unlike the $CD4^+$ populations, a.a.$CD8^+$ T cells showed a similar expression of TNF as liver-infiltrating $CD69^-$ $CD49a^-$ $CD45RO^+$ $CD8^+$ T cells. IFN-γ expression tended to be higher in the a.a.$CD8^+$ T cells. Moreover, granzyme A, B, and K were also detected in this population without *in vitro* stimulation (Fig. S5F). Finally, we investigated whether a.a.$CD8^+$ T cells were more prevalent in the livers of patients with AIH. Analysis of $CD8^+$ T cells from the same group of patients used for the $CD4^+$ T-cell study revealed that the $CD8^+$ T cells in the livers of patients with AIH showed significantly higher abundance of cells per mg of liver with the a.a. phenotype compared to controls (Fig. S5G).

Overall, we identified and validated $CD4^+$ $T_{RM}1$ cells and a.a.$CD8^+$ T cells in AIH livers as a potential source of TNF and IFN-γ, two of the proinflammatory cytokines we found to be associated with AIH.

AIH molecular-cellular network and its spatial distribution

Following the identification of the key AIH-related pathways and their cellular sources, we then aimed to integrate their relationships into a coherent interactome that enables the generation of hypotheses explaining the pathological immune network of AIH. To this end, we used CellChat[33] to infer intercellular communication probabilities by analyzing the expression of the preselected set of cytokine ligand–receptor pairs from the above analyses. *IL12*, which exhibited a positive correlation with disease severity in Fig. 1, was not included in this analysis due to low RNA counts. We differentiated between conventional IL-15 signaling (referred to as '*IL15* – (*IL15*RA+*IL2RB*+*IL2RG*)') and the trans-presentation of IL-15 ((*IL15*RA+*IL15*) – (*IL2RB*+*IL2RG*)).[34] The inferred interactions suggested that both $T_{RM}1$ cells and a.a.$CD8^+$ T cells can potentially respond to IL-15 and IL-7, which are produced by myeloid cells. In turn, $T_{RM}1$ and a.a.$CD8^+$ T cells could interact with myeloid cells by secreting TNF and IFN-γ and thus promote the pro-inflammatory phenotype of these innate cells. In addition, we found that TNF and its receptors can connect $T_{RM}1$ cells with a.a.$CD8^+$ T cells, suggesting potential support of $CD8^+$ T-cell survival by $CD4^+$ T cells. Next, $T_{RM}1$ and a.a.$CD8^+$ T cells were shown to potentially interact with hepatocytes through TNF, IFN-γ and FASLG, thus potentially contributing to tissue damage. Finally, hepatocytes secreting IL-7 and IL-15 could target the corresponding cytokine receptors on both $T_{RM}1$ and a.a.$CD8^+$ T cells, closing a potential vicious cycle, which may lead to chronic inflammation typical of AIH (Fig. 4A). A cell type-focused overview of these findings is provided in Fig. 4B.

To further support this AIH molecular-cellular network, we investigated cell neighborhoods within the spatial context using an independent cohort of patients with AIH. Specifically, we profiled the spatial distribution of 477 selected genes across six AIH liver biopsies and three control liver biopsies with unremarkable histopathological findings using the Xenium *In Situ* platform (10x Genomics) (spatial *in situ* RNA expression assay) (Fig. 4C). Dimensionality reduction of these data yielded 21 well-segregated clusters for AIH samples and 17 clusters for control samples, with a median of 50 genes detected per cell (Fig. S6A–C). We used the DEGs identified from our AIH atlas as a reference to annotate clusters and map cell types to their spatial localization (Fig. 4C and S6B,C). Compared to control livers, which exhibited clear zonation and minimal immune cell infiltration, AIH biopsies demonstrated disrupted zonation patterns and a marked increase in immune cell infiltration, including T cells, B cells, and myeloid cells (Fig. 4C). We next quantified the proportions of different immune and non-immune cell populations. $T_{RM}1$ and a.a.$CD8^+$ T cells were more abundant in AIH compared to control livers, while hepatocytes appeared to be diminished in AIH livers, as expected (Fig. S6D). Focusing on the different types of hepatocytes, their proportions varied between AIH and controls with a relative increase in hepatocytes with inflammatory features in AIH (Fig. S6E). In addition, more immune cells, including $T_{RM}1$ and a.a.$CD8^+$ T cells, were found adjacent to hepatocytes in AIH compared to control livers (Fig. S6F). At the hepatic-immune

donors excluded due to <80 $CD4^+$ T cells) (CITE-seq: n = 9; snRNA-seq: n = 5). Right: Heatmaps of selected canonical marker genes across all $CD4^+$ T-cell subclusters. (E) Left: Sub-clustering analysis of $CD8^+$ T cells including all 16 donors (CITE-seq: n = 10; snRNA-seq: n = 6). Right: Heatmaps of selected canonical marker genes across all $CD8^+$ T-cell subclusters. (F) Left: Sub-clustering analysis of hepatocytes based solely on snRNA-seq (n = 6), excluding hepatocytes from CITE-seq due to low recovery. Right: Heatmap of selected markers associated with zonation, inflammation, proliferation and regeneration. AIH, autoimmune hepatitis; CITE-seq, cellular indexing of transcriptomes and epitopes by sequencing; SLO, secondary lymphoid organ; snRNA-seq, single-nucleus RNA sequencing; UD, undefined; UMAP, uniform manifold approximation and projection.

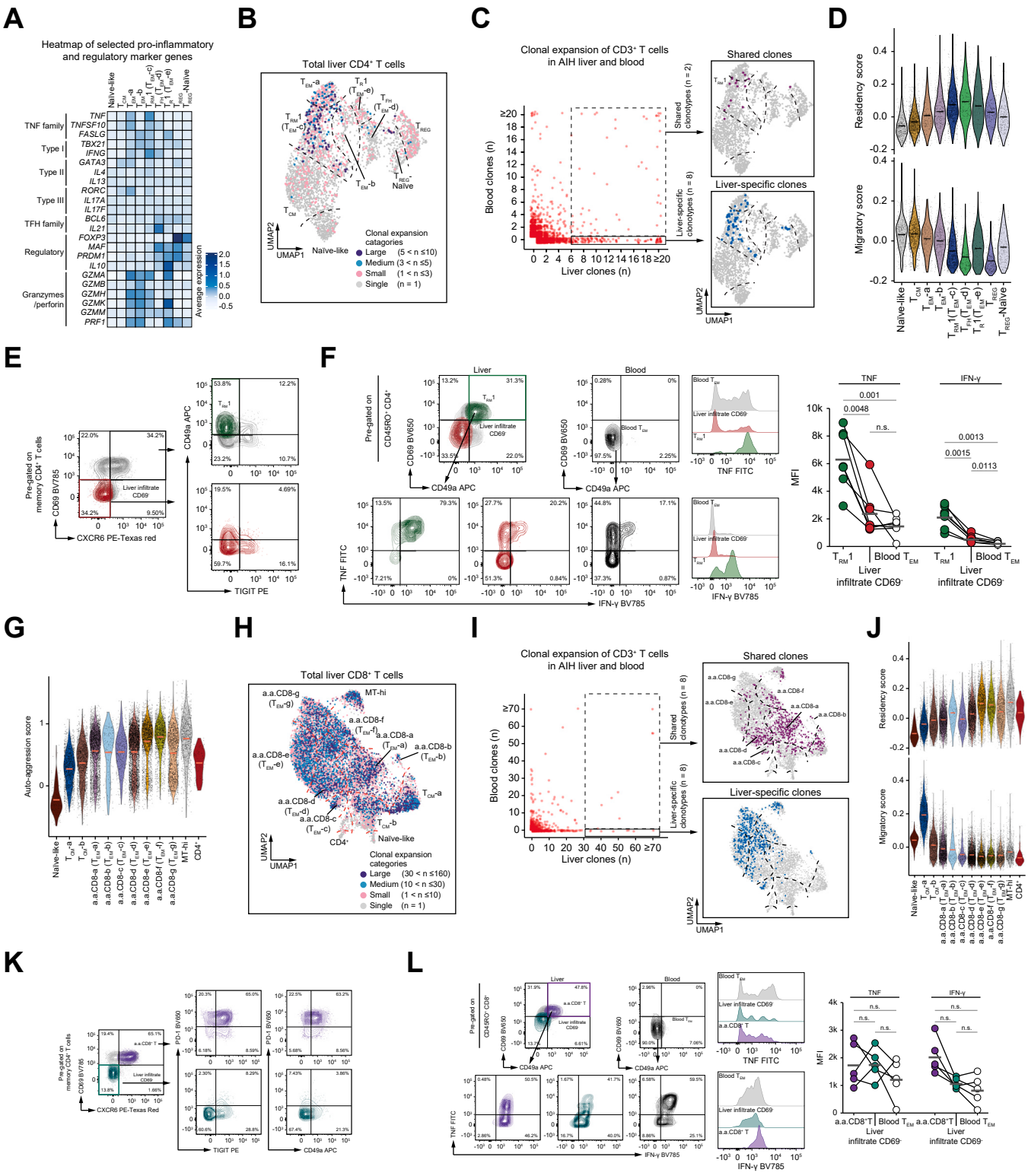

Fig. 3. Characterization of intrahepatic conventional T cells in AIH. (A) Heatmap of selected pro-inflammatory and regulatory marker genes across CD4$^+$ subclusters corresponding to those defined in Fig. 2D. Re-annotation of T_{EM}-c, T_{EM}-d, and T_{EM}-e as T_{RM}1, T_{FH}, and T_R1, respectively, based on their features. (B) UMAP showing the clonal expansion of CD4$^+$ T cells from CITE-seq data. Clonal expansion is determined by the total number of cells sharing the same clonotype. (C) Left: Clonal expansion of CD3$^+$ T cells, in livers and paired blood (liver CITE-seq: n = 3; paired blood CITE-seq: n = 3). The X-axis and Y-axis represent liver and blood clones, respectively, with clone counts ≥20 truncated to 20 for visualization. Right: UMAP of CD4$^+$ T cells highlighting highly abundant clones (frequencies of n ≥6) shared between the liver and blood (top), and liver-specific clones (bottom). (D) Migration and residency scores for all CD4$^+$ T-cell subclusters (CITE-seq: n = 9; snRNA-seq: n = 5). (E) Representative flow cytometry plots showing the expression of CD69 and CXCR6 on memory CD4$^+$ T cells in AIH livers. Distinct expression pattern of CD49a and TIGIT are used to identify T_{RM}1 cells. The gating strategy for memory CD4$^+$ T cells is shown in Fig. S4F. (F) Left: Representative flow cytometry plots showing TNF and IFN-γ expression patterns following *in vitro* stimulation in the indicated CD4$^+$ populations. CD45RO$^+$ CD4$^+$ T cells were pre-gated on TCRαβ$^+$

interface, we observed close adjacency between *TNF*-expressing $T_{RM}1$ cells and hepatocytes or $CD8^+$ T cells expressing *TNFRSF1A* or *TNFRSF1B* (Fig. 4D). Additionally, *IL7*-or *IL15*-expressing myeloid cells or hepatocytes were found in close proximity to $T_{RM}1$ and a.a.$CD8^+$ T cells expressing *IL7R or IL15R* (Fig. 4D). Targeting the same key players as indicated in Fig. 4A, namely $T_{RM}1$, a.a.$CD8^+$ T cells, myeloid cells and hepatocytes, we further analyzed the interaction probabilities of the selected ligand-receptor pairs, incorporating their spatial distances to calculate interaction probabilities (Fig. 4E). The resultant heatmap revealed various probable interactions similar to those shown in Fig. 4A; the majority of these interaction potentials were observed in AIH livers, but not in control livers (Fig. 4E). These findings provide further evidence of the potential interactions we proposed in AIH livers.

Functional validation of identified cellular interactions

Subsequently, we aimed to functionally validate some of the above-mentioned findings (Fig. 4). Based on the AIH cellular-molecular network and the cellular abundance of $T_{RM}1$ and a.a.$CD8^+$ T cells in AIH, we hypothesized that IL-7 and IL-15 play a role in inducing the proliferation of these cells. To functionally test this, we isolated and expanded both types of T cells from AIH liver biopsies and then exposed them to recombinant human IL-7 or recombinant human IL-15. IL-7 could induce the proliferation of $T_{RM}1$ cells in a dose-dependent manner, and IL-15 promoted the proliferation of both $T_{RM}1$ and a.a.$CD8^+$ T cells, also in a dose-dependent manner (Fig. 5A and S7A-F).

Next, we wondered whether the transcriptomic profile of a.a.$CD8^+$ T cells found in AIH livers translates into an a.a. function, *i.e*. MHC I-independent killing. To address this, we utilized a validated *in vitro* approach by co-culturing indicated populations with K562 target cells that lack MHC-I molecules without additional stimulation to test for auto-aggression,[21] and found that AIH liver-derived a.a.$CD8^+$ T cells displayed an MHC I-independent killing capacity (Fig. 5B). In contrast, we did not observe a reproducible a.a. function from liver $T_{RM}1$ cells nor from $CD8^+$ and $CD4^+$ T cells isolated from blood (Fig. 5B).

Although $T_{RM}1$ did not display direct a.a. properties, our interactome analysis identified both hepatocytes and a.a.$CD8^+$ T cells as targets of $T_{RM}1$ and of TNF, raising the possibility that $T_{RM}1$ may indirectly contribute to hepatocyte damage, potentially through TNF secretion. To explore this, we designed experiments to evaluate the impact of TNF pre-treatment on either the target cells or a.a.$CD8^+$ T cells, which, for the purpose of standardization, were generated by *in vitro* stimulation of blood-derived $CD8^+$ T cells with IL-15 as described.[21] Pre-treating IL-15-induced a.a.$CD8^+$ T cells with soluble TNF did not augment their a.a. function (Fig. 5C); however, pre-treating the target cells did enhance auto-aggression by a.a.$CD8^+$ T cells (Fig. 5D). Since $T_{RM}1$ cells can secrete TNF, we next pre-treated target cells with the culture supernatant of anti-CD3/anti-CD28-activated $T_{RM}1$ cells. We observed that this pre-treatment enhanced the a.a. effect exerted by blood-induced a.a.$CD8^+$ T cells. Of note, this increase in cytotoxicity was partially reversed by TNF blockade (Fig. 5E and S7G).

We next aimed to confirm some of these findings using primary human hepatocytes. We found that the pre-treatment of hepatocytes with the supernatant of activated $T_{RM}1$ cells increased the killing capacity of a.a.$CD8^+$ T cells, which was inhibited by TNF blockade (Fig. 5F and S7H).

Finally, we aimed to investigate the potential pathological effects of TNF on hepatocytes. TNF has been shown to upregulate ICAM1 in human epithelial cells.[35] Additionally, hepatocytes exposed to TNF upregulate ICAM1, facilitating close interactions with cytotoxic T cells in a MASH mouse model.[21] Therefore, we proposed that TNF exerts a similar effect in AIH. To assess this, we quantified TNF signaling activity in hepatocytes exploiting data from our atlas. Based on our AIH atlas dataset, using $CD8^+$ T cells as a positive control for TNF signaling, we classified hepatocytes into high and low TNF response groups (Fig. S7I). Differential gene analysis between the TNF-high and -low response groups revealed that several adhesion molecules, which facilitate physical interactions between hepatocytes and T cells, were upregulated in the TNF-high response group (Fig. S7J). Furthermore, a regression model revealed a significant positive association between TNF signaling pathway activity and the expression of adhesion molecules, including *ICAM1* (Fig. 5G). To further validate our findings in a spatial approach reflecting the *in vivo* conditions, we analyzed the spatial *in situ* RNA expression dataset with a particular focus on TNF receptor-positive hepatocytes in close proximity to TNF-producing cells (within 20 μm), including $T_{RM}1$,

TCRVα24-Jα18$^-$ live, singlet lymphocytes. Middle: Representative histograms showing the mean fluorescence intensity (MFI distribution) of TNF and IFN-γ across the indicated $CD4^+$ populations. Right: MFI quantification in 7 AIH donors. Each dot represents a single donor, with MFI levels of different populations from the same donor connected by lines. Grey lines represent mean values. Significant differences are determined by RM one-way ANOVA, Tukey's multiple comparisons test. (G) a.a. score for all $CD8^+$ T-cell subclusters (CITE-seq: n = 10; snRNA-seq: n = 6). Re-annotation of T_{EM}-a to -g as a.a.CD8 -a to -g respectively, based on their a.a. features. (H) UMAP showing the clonal expansion of $CD8^+$ T cells from CITE-seq data (n = 10). Clonal expansion is determined by the total number of cells sharing the same clonotype. (I) Left: Clonal expansion of $CD3^+$ T cells, in livers and paired blood (liver CITE-seq: n = 3; paired blood CITE-seq: n = 3). The X-axis and Y-axis represent liver and blood clones, respectively, with clone counts ≥70 truncated to 70 for visualization. Right: UMAP of $CD8^+$ T cells highlighting highly abundant clones (frequency ≥31) shared between liver and blood (top), and liver-specific clones (bottom). (J) Migration and residency scores for all $CD8^+$ T-cell subclusters (CITE-seq: n = 10; snRNA-seq: n = 6). (K) Representative flow cytometry plots showing the expression of indicated markers on memory $CD8^+$ T cells in AIH liver. The gating strategy for memory $CD8^+$ T cells is shown in Fig. S4F. (L) Left: Representative flow cytometry plots showing TNF and IFN-γ expression patterns in the indicated $CD8^+$ T-cell populations. $CD45RO^+$ $CD8^+$ T cells were pre-gated on TCRαβ$^+$ TCRVα24-Jα18$^-$ live, singlet lymphocytes. TNF and IFN-γ detection were performed after *in vitro* stimulation. Middle: Representative histogram showing the MFI distribution of TNF and IFN-γ across the indicated $CD8^+$ T-cell populations. Left and middle panels represent images from the same donor. Right: MFI quantification across five AIH donors. Each dot represents a single donor, with MFI levels of different populations from the same donor connected by lines. Grey lines represent mean values. Statistical differences are determined by repeated measures one-way ANOVA, Tukey's multiple comparisons test. Panels (A-D) and (G-J) were based on the AIH atlas, whereas panels (E,F,K,L) were based on the FACS dataset. Donors included in the FACS dataset represent an independent cohort. AIH, autoimmune hepatitis; CITE-seq, cellular indexing of transcriptomes and epitopes by sequencing; MFI, mean fluorescence intensity; snRNA-seq, single-nucleus RNA sequencing; T_{EM}, effector memory T cell; T_{FH}, T follicular helper cell; T_{R1}, type 1 regulatory T cell; T_{RM}, tissue-resident memory T cell; UMAP, uniform manifold approximation and projection.

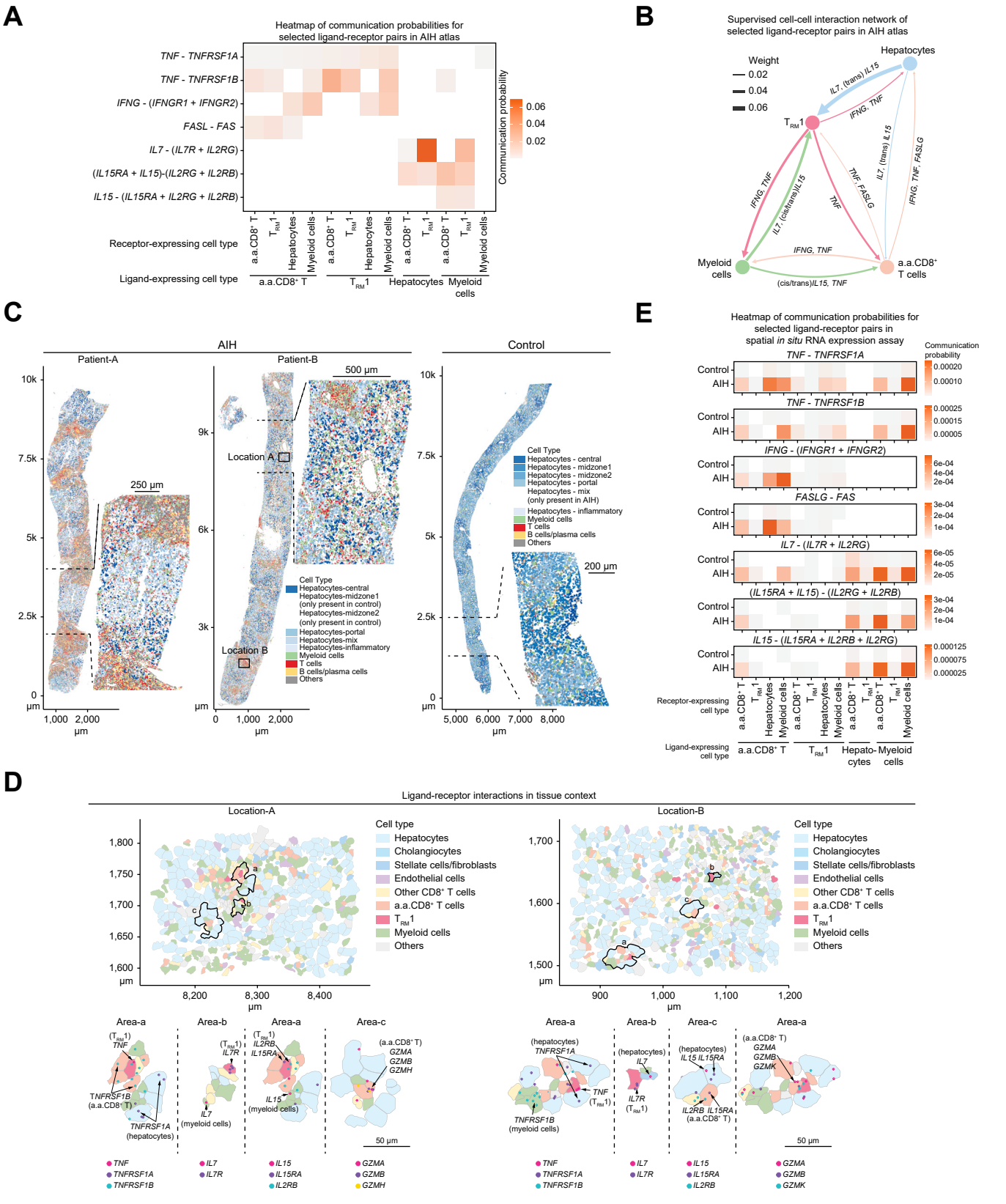

Fig. 4. Single cell-resolution spatially resolved interactome depicting interactions among $T_{RM}1$, a.a.CD8$^+$ T cells, myeloid cells, and hepatocytes in the livers of patients with AIH. (A) Heatmap showing the significant (*p* adjusted <0.05, one-sided permutation test) communication probability values by CellChat of selected ligand-receptor pairs and the interacting cell types, based on gene expression from the AIH atlas. (B) Supervised interaction network of indicated players and selected ligands, based on data from (A). Cytokines of source cell type (line color) are labeled. Weight equals the sum of communication probability. (C) Representative spatial

a.a.CD8$^+$ T cells and myeloid cells. As controls, we included hepatocytes without TNF receptor expression in close proximity to TNF-secreting cells. Consistent with the AIH atlas analysis, both *ICAM1* and *CDH1* mRNA were highly expressed in hepatocytes, presumably reflecting their response to TNF (Fig. 5H and S8A). Our findings suggest a potential mechanism of TNF action on hepatocytes, involving the upregulation of adhesion molecules, including ICAM1, to induce a.a.CD8$^+$ T cell/T_{RM}1-mediated cytotoxicity in the AIH liver.

In summary, our data revealed a molecular and cellular network that could contribute to the pathogenesis of AIH. While myeloid and hepatocyte-derived IL-7 and IL-15 may have accounted for the accumulation of T cells in the liver, the cytokine TNF, which can derive from liver T_{RM}1 cells, enhanced the cytotoxic activity of a.a.CD8$^+$ T cells by upregulating adhesion molecules on hepatocyte targets.

Anti-TNF treatment with infliximab in patients with newly diagnosed AIH

In parallel, we investigated one of the suspected key nodes of AIH pathogenesis, TNF, as a therapeutic target in a phase IIa, proof-of-concept trial testing infliximab (IFX) as an alternative to conventional corticosteroid induction therapy for a distinct cohort of patients with newly diagnosed AIH (Trial Registration: EudraCT No. 2017-003311-19). In total, 12 patients were enrolled in the trial, nine of whom could be analyzed (Fig. 6B). The primary endpoint – defined as complete biochemical remission (*i.e.* normalization of ALT, AST and IgG) after 24 weeks (6 months) of treatment with IFX was reached by 2/12 patients (17%, Fig. 6A). Nine patients were included in the final analysis cohort (n = 8 who completed all scheduled infusions and n = 1 who received 6/8 doses). 9/9 patients (100%) exhibited transaminases ≤2x the upper limit of normal after 6 months of treatment. IFX significantly decreased ALT and AST levels by 92.7% and 65.5%, respectively, after six months (Fig. 6C,D, percentages/*p* values based on the linear mixed-effects model analyses [n = 12], p <0.0001 for reductions of ALT and AST; see Table S2 for observed relative reductions of the final analysis cohort [n = 9]). Complete normalization of AST and ALT was achieved in 6/9 and 5/9 patients (67% and 56%), respectively.

Trial outcomes were compared with standard-of-care corticosteroid induction therapy for AIH using prospectively collected data from 24 patients in the R-LIVER registry,[9] treated at the same center. Propensity score matching was applied to the baseline covariates age, ALT, mHAI, IgG and bilirubin, with sex and histologically confirmed advanced fibrosis or cirrhosis (F3-4) specified as exact-matching variables. Detailed baseline characteristics are outlined in Table 1. Further analysis revealed no significant differences regarding ALT reduction between the treatment groups (p for interaction group × time point [$p_{group\times time}$] = 0.68, Fig. 6E). The rate of complete normalization of serum transaminases was similar in both cohorts (12/24 patients [50%] in the SoC cohort *vs.* 5/9 patients [56%] in the IFX cohort, p = 1.0, Fig. 6E and S9A). IgG normalization was observed more frequently in the SoC cohort (18/24 patients [75%] *vs.* 3/9 patients [30%] receiving IFX in the clinical trial, p = 0.04, Fig. 6F), though IgG reduction did not differ significantly between groups ([$p_{group\times time}$] = 0.051). The composite endpoint of normalized AST, ALT and IgG after 6 months was achieved in 10/24 patients (41.7%) in the SoC cohort and 2/12 patients (17%) in the cohort receiving IFX (p = 0.26).

Liver stiffness measurement by transient elastography reflects inflammation and fibrosis in AIH.[36] The impact of IFX treatment on liver stiffness was hence evaluated as a secondary endpoint (Fig. 6G). After 6 months, IFX led to a significant reduction of liver stiffness by 7.1 kPa on average in the linear mixed-effects model (p = 0.002). In the control cohort receiving SoC, available data from 13 patients with measurements at both time points revealed a mean reduction of 5.2 kPa (p = 0.005). The linear mixed-effects model revealed no significant differences between groups with regard to liver stiffness ($p_{group\times time}$ = 0.46).

Given the considerable known side effects associated with the current steroid-based standard induction therapy,[4–7] the clinical trial assessed both weight/BMI, as well as reports of the patients' HRQoL. Changes in BMI did not differ significantly between groups ($p_{group\times time}$ = 0.52, Fig. 6H). Detailed information on primary and secondary outcome measures, as well as on further laboratory findings, is provided in Table S2. At month 6, minor improvements in the mean difference from baseline were observed in the majority of subcategories of the SF-36 health survey (see Fig. S9B and Table S3 for detailed information on HRQoL collected within the clinical trial).

During the 6-month treatment phase with IFX (Fig. 6A), a total of 37 AEs of any kind were reported. All AEs were classified as mild or moderate. All AEs for which a possible relationship to study participation could not be excluded had resolved by the end of the observation period. With 9 out of 37 AEs (24%), gastrointestinal symptoms (such as heartburn/abdominal pain, nausea, vomiting) were the most frequently observed events. Two patients experienced serious AEs, both assessed as of questionable relation to the trial treatment: one patient was admitted to the emergency room for symptoms of marked arthralgia 24 h after their second dose of IFX associated with a mild acute upper respiratory tract viral infection not requiring hospitalization. This patient, whose ALT levels had already fallen by >60% compared to baseline, subsequently withdrew study consent. The second patient developed two consecutive episodes of febrile pyelonephritis after 6 out of 8 planned IFX doses and received inpatient antibiotic treatment. The patient had already achieved complete biochemical remission at the onset of the SAE, so further administration of the study drug was deemed inappropriate in this

distribution of cells from two active AIH livers and one control liver, color-coded by cell type (myeloid cells: macrophages, monocytes, Kupffer cells, granulocytes and dendritic cells; T cells: CD4$^+$ and CD8$^+$ T cells). Magnified views provide detailed depictions of cellular distributions. (D) Zoomed-in views of the spatial distribution of cells from the two areas indicated in (C). Below: magnified spatial distribution of cells, with selected ligand and receptor RNA expression overlaid. (E) Heatmap showing the significant (p adjusted <0.05, one-sided permutation test) communication probability values by CellChat of selected ligand-receptor pairs and the interacting cell types at distances up to 50 μm, based on *spatial in situ* RNA expression dataset. Donors included in the spatial *in situ* RNA expression dataset represent an independent cohort. AIH, autoimmune hepatitis; a.a.CD8+, auto-aggressive CD8$^+$ T cell; T_{RM}1, tissue resident-like type 1 memory cell.

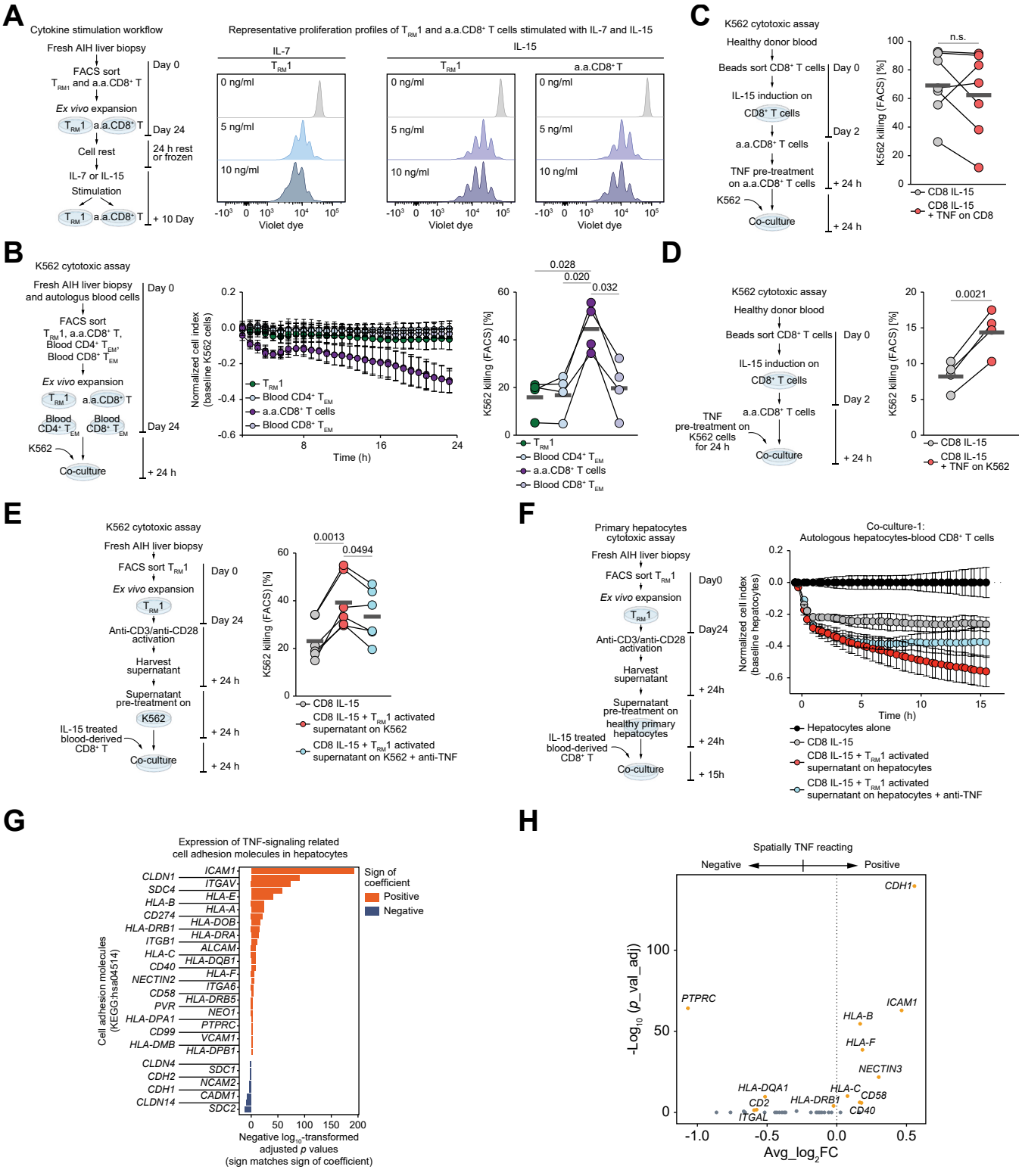

Fig. 5. $T_{RM}1$-derived TNF licenses the killing capacity of a.a.CD8$^+$ T cells. (A) Left: Schematic representation of the cytokine stimulation workflow. Right: Representative CellTrace Violet histograms showing proliferation of AIH liver-derived $T_{RM}1$ and a.a.CD8$^+$ T cells in response to IL-7 and IL-15 stimulation. (B) Left: Schematic representation of the K562 cytotoxicity assay. Middle: Real-time cell impedance analyses performed over 24 h showing auto-aggressive activity of AIH liver-derived a.a.CD8$^+$ T cells, $T_{RM}1$ cells, and paired blood CD4$^+$ T_{EM} and CD8$^+$ T_{EM} cells against K562 target cells (AIH patient, n = 1). Cytotoxicity was assessed in the absence of external stimulation and quantified using xCELLigence. Each dot represents the mean of triplicates for the indicated condition at the specified time point, with bars indicating the standard deviation. Right: Auto-aggressive activity of AIH liver-derived a.a.CD8$^+$ T cells, $T_{RM}1$ cells, and paired blood CD4$^+$ T_{EM} and CD8$^+$ T_{EM} cells against K562 target cells (AIH patients, n = 4). Cytotoxicity was quantified using flow cytometry. Each dot represents a single donor. Grey lines represent mean values. Significant differences are determined by repeated measures one-way ANOVA, Tukey's multiple comparisons test. (C) Left: Schematic

circumstance. Having already received 75% of the planned doses, the patient was included in the endpoint analyses. Two patients were prematurely excluded from further study participation after one and two doses, respectively, as they fulfilled the definition of insufficient response by the very strict safety rules of the phase IIa trial protocol (requiring premature study discontinuation in case of an increase in transaminases >20% over baseline within the first 4 weeks of treatment). They also received steroid-based rescue therapy.

In summary, this trial demonstrates the efficacy of the anti-TNF antibody infliximab as a steroid-free therapy in newly diagnosed AIH, confirming TNF as a key node of the pathogenic AIH immune network.

Discussion

We provide a description of a comprehensive and cohesive cellular and molecular network which might be responsible for the thus far elusive pathogenesis of AIH. In addition, this data set can be used as a resource for the identification of new targets for immunotherapeutic interventions in AIH. To obtain this resource, we integrated several mutually corroborating omics techniques, computational modelling, and functional assays from distinct cohorts of patients with AIH. Unsupervised analysis identified several cytokines associated with type I immune responses, particularly TNF, IL-12, and IFN-γ, and their downstream signaling pathways (RELA, NF-κB, JAK-STAT), correlating with the degree of liver inflammation and damage (Fig. 1). This finding is in line with previous reports of elevated plasma levels of cytokines in patients with AIH,[37,38] in particular of TNF, IL-12, and IFN-γ, which decline in disease remission.[37] We generated a comprehensive single-cell atlas (Fig. 2), profiling immune and non-immune cell populations, *i.e.* $CD4^+$ T cells, $CD8^+$ T cells, myeloid cells, hepatocytes and cholangiocytes. This AIH atlas is in alignment with published reports of healthy and diseased human livers in representing the major cell types and typical organ features like zonation,[26,39,40] but in addition, it establishes a unique representation of AIH-specific liver cell characteristics.

The AIH atlas confirmed our previous observation of an abundance of TNF-producing Th1 cells in AIH livers,[19] but also suggested a critical role of liver-resident $CD4^+$ $T_{RM}1$ cells as producers of TNF (Fig. 3). These hepatic $T_{RM}1$ cells matched a previously described phenotype.[18] The presence of $T_{RM}1$ cells is not unique to AIH, as these cells have also been detected in livers with less inflammatory activity, albeit at lower abundance. The TNF-producing $T_{RM}1$ cells were clonally expanded in the livers of patients with AIH. However, the identification of the specific activating antigens requires further investigation. Autoreactive $CD4^+$ T cells have previously been identified in the blood of anti-SLA/LP auto-antibody-positive patients with AIH.[16,17,41] These autoreactive T cells mainly seemed to represent *IL21*-positive T_{FH} cells. Our study did not assess TCR specificity, limiting direct comparison with these findings. However, liver T_{FH} cells in our dataset are characterized by *PDCD1*, *CTLA4*, *TIGIT*, and *ICOS*, as well as by *TOX2*, *NR3C1*, and *MAF* genes, markers that were previously described for autoreactive $CD4^+$ T cells.[16,17] This suggests a potential link between what we identified here as liver T_{FH} and blood autoreactive $CD4^+$ T cells and calls for further investigation in this regard.

Our AIH atlas also revealed a substantial clonal expansion of $CD8^+$ T cells in AIH livers. This cell population appears to be heterogeneous, with some of the clusters exhibiting a T_{RM} signature and partially exclusive clonal representation in the liver (Fig. 3). Note that a $CD8^+$ T-cell population with similar memory and residency markers was found to be significantly increased in the livers of patients with AIH, strongly correlating with disease severity.[20] Intriguingly, our atlas revealed that this population displays an a.a. state (Fig. 3) and function, including cytotoxicity independent of TCR-stimulation (Fig. 5). This is consistent with the recent report indicating a pathogenic role of a.a.$CD8^+$ T cells in MASH,[21] suggesting that a.a.$CD8^+$ T cells might be of pathogenic relevance in different liver diseases.

representation of the K562 cytotoxicity assay. Right: Auto-aggressive activity of IL-15-treated blood $CD8^+$ T cells (*i.e.* CD8 IL-15) pre-treated without or with TNF, against K562 target cells. Cytotoxicity was quantified by flow cytometry. Blood $CD8^+$ T cells were derived from healthy donors (n = 7). Each dot represents a single donor. Grey lines represent mean values. Statistical difference is determined by paired t-test. (D) Left: Schematic representation of the K562 cytotoxicity assay. Right: Auto-aggressive activity of IL-15-treated blood $CD8^+$ T cells against K562 cells pre-treated without or with TNF. Cytotoxicity was quantified by flow cytometry. Blood $CD8^+$ T cells were derived from healthy donors (n = 4). Each dot represents a single donor. Grey lines represent mean values. Significant difference is determined by paired t-test. (E) Left: Schematic representation of the K562 cytotoxicity assay. Right: Auto-aggressive activity of IL-15-treated blood $CD8^+$ T cells against K562 target cells (grey), K562 cells pre-treated with supernatant from anti-CD3/anti-CD28 activated $T_{RM}1$ cells, in the absence (red) or presence (blue) of anti-TNF. Cytotoxicity was quantified by flow cytometry. Blood $CD8^+$ T cells were derived from healthy donors (n = 6) and $T_{RM}1$ cells were derived from AIH livers (n = 4). Supernatant from $T_{RM}1$ cells from two AIH donors was cultured with $CD8^+$ T cells from one healthy donor each. Supernatant from $T_{RM}1$ cells from two additional AIH donors was cultured with $CD8^+$ T cells from two healthy donors each, resulting in a total of six independent measurements. Each dot represents a co-culture condition. Grey lines represent mean values. Significant differences are determined by repeated measures one-way ANOVA, Tukey's multiple comparisons test. (F) Left: Schematic representation of human primary hepatocyte cytotoxicity assay. Right: Real-time cell impedance analysis over 15 h showing auto-aggressive activity of autologous blood $CD8^+$ T cells against primary human hepatocytes under the indicated conditions. Hepatocytes were co-cultured with $CD8^+$ T cells (grey), or pre-treated with supernatant from anti-CD3/anti-CD28-activated $T_{RM}1$ cells in the absence (red) or presence of anti-TNF (blue). Baseline hepatocytes are shown in black. Auto-aggression was assessed by hepatocyte viability and quantified using xCELLigence. Primary hepatocytes and autologous blood $CD8^+$ T cells were obtained from one healthy donor, and $T_{RM}1$ cells were isolated from the liver of one AIH donor. Each dot represents the mean of triplicates for the indicated condition at the specified time point, with bars indicating the standard deviation. (G) TNF signaling pathway score (see Fig. S7I), based on the AIH atlas, indicating the expression of cell adhesion molecules (KEGG:hsa04514) in hepatocytes using a hurdle regression model. Depicted are significant (p <0.05) negative $\log_{10}$-transformed p values multiplied by the sign of the coefficient. (H) Volcano plot of spatial *in situ* RNA expression data showing differentially expressed cell adhesion genes between TNF receptor positive and negative cells within 20 μm of TNF-producing cells. TNF receptor-positive cells are defined by the expression of either *TNFRSF1A* or *TNFRSF1B*. Cells used in panels (A-E) derived from the same donors as the FACS dataset in Fig. 3. The gating strategies for $T_{RM}1$ and a.a.$CD8^+$ T cells are described in Fig. S4F followed by Fig. 3E and K, respectively. Paired blood $CD4^+$ and $CD8^+$ T_{EM} cells were identified using the same gating strategies described in Fig. S4F for $CD4^+$ and $CD8^+$ memory subsets, respectively. AIH, autoimmune hepatitis; a.a.$CD8^+$, auto-aggressive $CD8^+$; MFI, mean fluorescence intensity; T_{EM}, effector memory T cell; $T_{RM}1$, tissue resident-like type 1 memory cell.

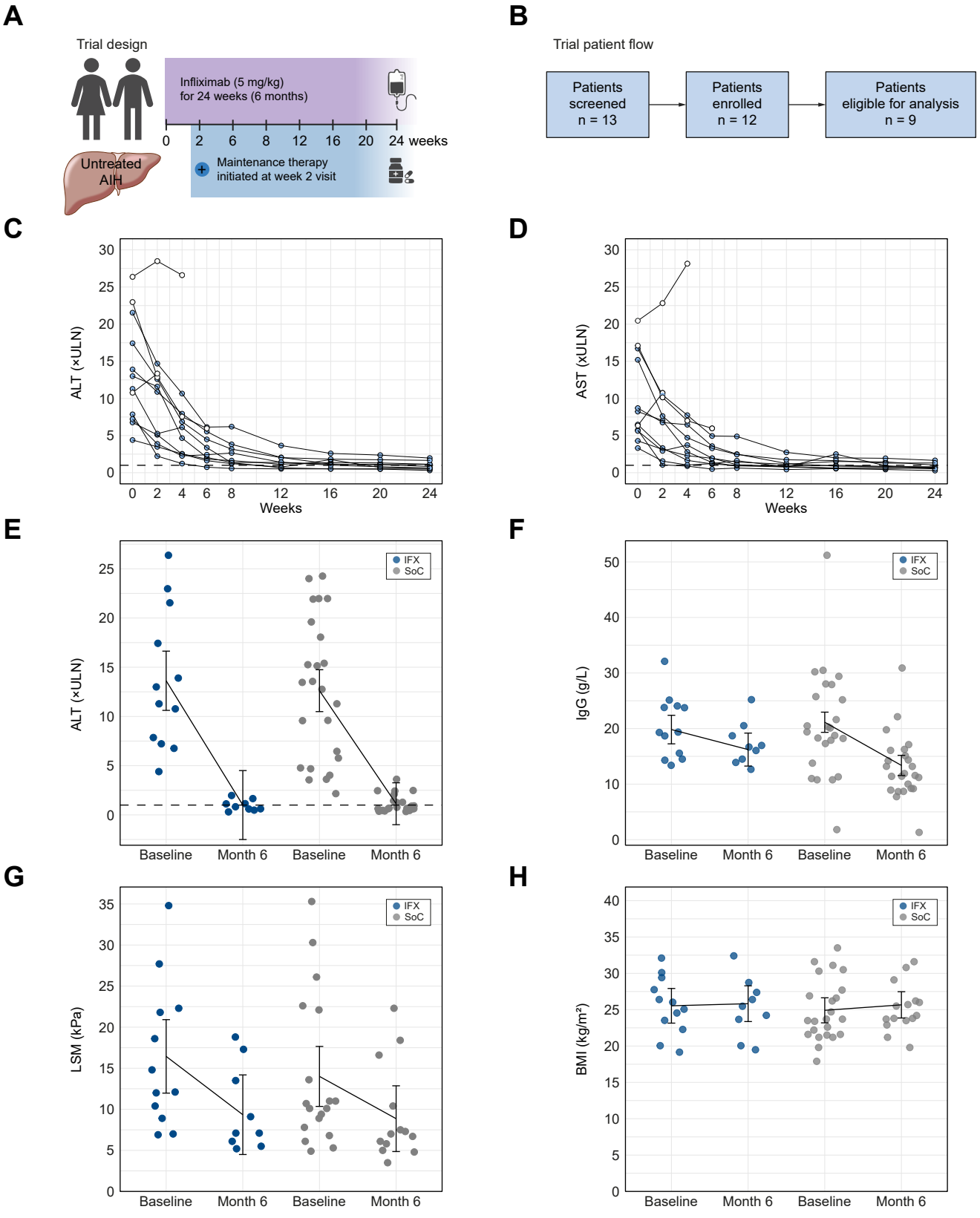

Fig. 6. Steroid-free treatment with infliximab ameliorates hepatic inflammation in patients with previously untreated AIH. (A) Trial design (AIH-MAB): n = 12 patients were enrolled to receive infliximab (5 mg/kg) for 24 weeks and were started on maintenance therapy commencing after the week 2 visit. (B) Patient flow within AIH-MAB. (C,D) Individual ALT (C) and AST (D) levels (xULN) over the course of the 24-week experimental treatment. Light circles depict patients who were excluded from the primary analysis (n = 3). (E,F) Comparison of ALT (xULN, (E)) and IgG (g/L, (F)) between baseline and month 6 in patients receiving IFX (individual values shown as purple dots, n = 12) or standard care (n = 24, orange dots). (G,H) Comparison of liver stiffness (kPa, (G)) and BMI (kg/m2, (H)) between baseline and month 6,

Table 1. Baseline patient characteristics of the AIH-MAB cohort receiving IFX (n = 12) and the matched prospective control cohort receiving SoC (n = 24).

	IFX (n = 12)	SoC (n = 24)	SMD
Female, n (%)	9 (75)	18 (75)	0
Age at diagnosis, years	36 (18-63)	41 (22-62)	-0.205
mHAI	9 (5-15)	10 (4-14)	-0124
Simplified AIH score	7 (5-8)	7 (4-7)	0.383
Advanced fibrosis/cirrhosis, n (%)	3 (25)	6 (25)	0
Liver stiffness (kPa)	13.5 (6.9-34.8)	10.4 (4.9-35.3)[1]	0.271
BMI (kg/m^2)	25.6 (19.2-32.1)	23.7 (17.9-33.5)[2]	0.150
ALT xULN	12.15 (4.40-26.37)	13.11 (2.16-24.26)	-0.140
AST xULN	7.36 (3.32-20.46)	16.49 (4.26-28.46)	-0.961
IgG (g/L)	19.3 (13.4-32.1)	19.8 (1.81-51.2)	-0.059
GGT (U/L)	120 (41-331)	146 (50-422)	-0.287
ALP (U/L)	131 (67-343)	130 (59-396)	0.026
Total bilirubin (mg/dl)	1.1 (0.5-4.7)	1.2 (0.4-3.0)	-0.025
Albumin (g/dl)	36.6 (32.2-41.7)[3]	37.0 (25.6-46.1)[4]	-0.119
INR	1.1 (1.0-1.1)[5]	1.1 (0.9-1.5)	-0.576
ANA, n (%)[6]	12 (100)	21 (88)	0.534
SMA, n (%)[6]	7 (58)	10 (42)	0.338
LKM, n (%)	1 (8)	0	0.426
SLA/LP, n (%)	0 (0)	1 (4)	-0.295

Continuous variables = medians (range).
Group comparisons = SMD.
AIH, autoimmune hepatitis; ALP, alkaline phosphatase; ALT, alanine aminotransferase; ANA, antinuclear antibodies; AST, aspartate aminotransferase; GGT, gamma-glutamyl transferase; IFT, immunofluorescence testing; IFX, infliximab; INR, international normalized ratio; LKM, liver kidney microsomal antibodies; mHAI, modified histology activity index; SLA/LP, soluble liver antigen/liver pancreas antibodies; SMA, smooth muscle antibodies; SMD, standardized mean difference; SoC, standard of care; ULN, upper limit of normal.
[1]Data available for 18 patients.
[2]Data available for 23 patients.
[3]Data available for 9 patients.
[4]Data available for 22 patients.
[5]Data available for 10 patients.
[6]Considered positive if IFT ≥1:160.

Our data do not exclude a role for antigen-specific CD4$^+$ and CD8$^+$ T cells. Notably, we observed upregulation of MHC I and II molecules in hepatocytes, potentially in response to TNF stimulation. Thus, a conceivable hypothesis is that self-reactive T cells represent the initial triggers and effectors of the inflammatory reaction in AIH, and that, once the immune response is established, MHC-independent CD8$^+$ T-cell–mediated killing could further escalate the response. Further efforts are needed to dissect the relationship between self-reactive, non-self-reactive and a.a. T cells in the pathogenesis of AIH.

Having found clonal expansion of both $T_{RM}1$ and a.a.CD8$^+$ T cells in the liver of patients with AIH, we searched for potential drivers of this expansion. IL-7 has been shown to promote the proliferation of naive and T_{EM} cells.[42] Consistent with this, our computational modelling identified interactions between hepatocytes and myeloid cells with $T_{RM}1$ cells via IL-7 and IL-7R. Furthermore, *in vitro* functional validation demonstrated that AIH liver-derived $T_{RM}1$ cells can proliferate in response to IL-7 in a dose-dependent manner (Fig. 5). Similarly, IL-15, also mainly produced by myeloid cells and hepatocytes, could drive the proliferation of AIH liver-derived $T_{RM}1$ and a.a.CD8$^+$ T cells in a dose-dependent manner (Fig. 5). However, proliferation occurs only after 4 days of *in vitro* stimulation, consistent with the observation that short-term IL-15 stimulation induces an a.a. phenotype, while long-term stimulation promotes proliferation.[21,43,44] Hepatocytes seemed to actively participate in AIH pathogenesis, not only by producing IL-7 and IL-15, but also by upregulating *IL32* expression, which has been shown to induce TNF expression in human monocytic cells,[45] suggesting that hepatocytes are not just passive victims in AIH.

At least to a certain extent, the inflammatory and activated phenotype of hepatocytes seemed to be induced by TNF derived from expanded CD4$^+$ $T_{RM}1$ cells in livers of patients with AIH, as inferred from interactome analysis and confirmed by spatial Xenium analysis (Fig. 4). While TNF signaling is linked to both hepatocyte proliferation and apoptosis,[46,47] we also observed upregulation of integrins, such as *ICAM1*, *ITGAV* and *ITGB1,* in hepatocytes that appeared to exhibit active TNF signaling (Fig. 5). This observation correlates well with data showing that TNF exposure upregulates ICAM1 in mouse hepatocytes and human vascular epithelial cells.[21,35] Moreover, our *in vitro* study showed that pre-treatment of target cells with TNF enhanced the killing capacity of a.a.CD8$^+$ T cells. Considering this and previous published data in mouse models,[21] we speculate that this effect was due to the enhanced expression of ICAM1, which increased the contact between hepatocytes and a.a.CD8$^+$ T cells, resulting in increased hepatocyte killing. These data also affirm the idea that hepatocytes not only serve as the primary targets of the immune-mediated damage, but also play an active role in

separated by treatment (IFX *vs.* SoC). Black lines and error bars indicate respective EMMs and their respective 95% CIs of the linear mixed-effects model analyses.
AIH, autoimmune hepatitis; ALT, alanine aminotransferase; AST, aspartate aminotransferase; EMMs, estimated marginal means; IFX, infliximab; SoC, standard of care; xULN, times the upper limit of normal.

sustaining the immune response by responding to immunological insults. Accordingly, hepatocytes upregulated the expression of MHC II molecules enabling them to interact with $CD4^+$ T cells, in particular with TNF-producing $T_{RM}1$ cells.

In addition to identifying TNF as a central node in the AIH inflammatory network, we conducted a phase IIa clinical study targeting TNF with the anti-TNF antibody IFX, which proved effective in ameliorating hepatic injury (Fig. 6), further adding to the validity of our analysis. More significantly, this trial marks the first demonstration that steroid-free induction therapy for acute AIH is both viable and achievable. While not all patients responded rapidly to IFX, the overall response rate was high, as indicated by the clear reduction of transaminases and the similar rate of transaminase normalization at month 6, compared to the SoC control group. This proof-of-concept clinical trial naturally has limitations. Firstly, it was performed in a small number of patients. To address that limitation, we have applied the linear mixed-effects model, which provides a conservative and statistically appropriate framework for small, incomplete longitudinal datasets such as ours. Secondly, despite thorough matching for various parameters that might have influenced the therapeutic response,[48] this was not a randomized blinded trial and thus its efficacy as an alternative standard therapy requires further validation. As this trial was not focused on safety outcomes, the cohort size was not sufficient to detect rare AEs such as IFX-induced liver injury. However, existing data indicate that IFX-associated hepatotoxicity is uncommon, usually mild and reversible after treatment discontinuation,[49] and safety concerns regarding IFX in the context of AIH have not been reported so far.[50,51] Nevertheless, larger controlled studies will be required to confirm the safety profile of IFX in AIH. In large cohort studies on the treatment of chronic inflammatory bowel disease, long-term comparisons of corticosteroids with anti-TNF therapies revealed an increased mortality rate and reduced quality of life in the steroid group.[52,53] These findings underscore the need to further explore corticosteroid-free treatment strategies for AIH.

This very cautiously designed trial protocol may even have underestimated the strength of the treatment effect. Firstly, the two patients excluded early in the trial who did not respond rapidly to the treatment may have required more time for the immune intervention to take effect. To handle delayed responses, adding a short-term steroid treatment in combination with IFX (as is routine in other applications like inflammatory bowel disease) might be a feasible solution in respective cases without lasting untoward effects. Secondly, in line with the current consensus on a complete biochemical remission, the primary endpoint was complete normalization of both transaminases and IgG after six months. However, this definition of remission is controversial, and it remains unclear whether normalization of IgG is of any prognostic significance. Indeed, recent studies indicated that only elevated aminotransferases, but not IgG, were associated with impaired prognosis,[48,54] which further underscores the relevance of the transaminase reduction observed in the present trial. Our results are an encouraging signal for patients affected by AIH, particularly for those with relative contraindications (such as diabetes or established osteoporosis) to corticosteroid therapy.

Overall, these computational, experimental and clinical data reveal the pathogenic AIH network at a hitherto unprecedented depth, providing a resource for the identification of therapeutic targets in AIH. Although we focused on TNF here, which we identified as a major node in the AIH network, additional potential drug targets may be derived from this dataset. After decades of solely steroid-based induction therapy, these data may usher in a new era of immunotherapy in AIH.

Affiliations

[1]*Hamburg Center for Translational Immunology (HCTI), University Medical Center Hamburg-Eppendorf (UKE), Hamburg, Germany;* [2]*I. Department of Medicine, University Medical Center Hamburg-Eppendorf (UKE), Hamburg, Germany;* [3]*Institute for Inflammation and Carcinogenesis, University Medical Center Hamburg-Eppendorf (UKE), Hamburg, Germany;* [4]*Center for Biomedical AI (bAIome), University Medical Center Hamburg-Eppendorf (UKE), Hamburg, Germany;* [5]*Institute of Molecular Immunology and Experimental Oncology, School of Medicine, Technical University of Munich (TUM), Munich, Germany;* [6]*II. Department of Medicine, University Medical Center Hamburg-Eppendorf (UKE), Hamburg, Germany;* [7]*Max Delbrück Center for Molecular Medicine in the Helmholtz Association (MDC), Berlin, Germany;* [8]*Institute of Medical Biometry and Epidemiology, University Medical Center Hamburg-Eppendorf (UKE), Hamburg, Germany;* [9]*Departamento de Biología, Facultad de Ciencias, Universidad de Chile, Santiago, Chile;* [10]*Faculty of Medicine, Universidad de los Andes, Chile;* [11]*Centro Científico y Tecnológico de Excelencia Ciencia & Vida, Fundación Ciencia & Vida, Santiago, Chile;* [12]*Facultad de Medicina, Universidad de Chile, Santiago, Chile;* [13]*Institute of Pathology, University Medical Center Hamburg-Eppendorf (UKE), Hamburg, Germany;* [14]*Institute of Medical Systems Bioinformatics, Center for Molecular Neurobiology (ZMNH), University Medical Center Hamburg-Eppendorf (UKE), Hamburg, Germany;* [15]*III. Department of Medicine, University Medical Center Hamburg-Eppendorf (UKE), Hamburg, Germany;* [16]*Institute for Immunology, University Medical Center Hamburg-Eppendorf (UKE), Hamburg, Germany;* [17]*Department of General, Visceral and Thoracic Surgery, University Medical Center Hamburg-Eppendorf (UKE), Hamburg, Germany;* [18]*Department of Clinical Medicine, Aarhus University, Denmark;* [19]*Department of Pathology, Aarhus University Hospital, Denmark;* [20]*German Center for Child and Adolescent Health (DZKJ), Partner Site Hamburg, University Medical Center Hamburg-Eppendorf (UKE), Hamburg, Germany;* [21]*Martin Zeitz Center for Rare Diseases, University Medical Center Hamburg-Eppendorf (UKE), Hamburg, Germany*

Abbreviations

AE, adverse events; AIH, autoimmune hepatitis; ALT, alanine aminotransferase; AST, aspartate aminotransferase; a.a., auto-aggressive; CITE-seq, cellular indexing of transcriptomes and epitopes by sequencing; DEGs, differentially expressed genes; HRQoL, health-related quality of life; IFX, infliximab; MASH, metabolic dysfunction-associated steatohepatitis; mHAI, modified hepatic activity index; PBC, primary biliary cholangitis; scTCR-seq, single-cell T-cell receptor sequencing; snRNA-seq, single-nucleus RNA sequencing; SoC, standard of care; T_{CM}, central memory T cell; T_{EM}, effector memory T cell; T_{REG}, $FOXP3^+$ regulatory T cell; T_{RM}, tissue-resident memory T cell; $T_{RM}1$, tissue resident-like type 1 memory cell.

Financial support

This study was supported by the German Research Foundation ("Deutsche Forschungsgemeinschaft") through funding of the collaborative research centers ("Sonderforschungsbereiche"/SFB) CRC 841 and CRC 1700 (project number 530990199). J.P.W. was supported by the German Liver Foundation ("Deutsche Leberstiftung", project number S0163/10182/2023) and the "iDfellows Hamburg Clinician Scientist Programme" in Infectious Diseases (German Research Foundation, funding code 493624519). C.Ki. was supported by the "iDfellows Hamburg Clinician Scientist Programme" in Infectious Diseases (German Research Foundation, funding code: 493624519). J.Ha. was supported by the German Federal Ministry of Education and Research (project number 01EO2106)

and German Research Foundation (project funding HA 8440/3-1). N.K. and S.B. were funded by CDL FLIGHT of the University of Hamburg and SFBs 1700 and 1192. M.R.B. and S.N. were funded by Centro Ciencia & Vida FB210008 from ANID and Grant from ANID FONDECYT 1230183, and CONICYT/FONDEQUIP EQM220027. C.S. was supported by the Helmut and Hannelore Greve Foundation and the YAEL Foundation.

Conflicts of interest

Authors declare that they have no conflict of interests. NG reports financial support from F. Hoffmann-La Roche and GSK via UKE. These are outside the submitted work.

Please refer to the accompanying ICMJE disclosure forms for further details.

Authors' contributions

Yang Xu, Jan Philipp Weltzsch and Christoph Kilian collaboratively conceived, designed and carried out the experiments and clinical trial, analyzed the data, provided critical intellectual input, prepared the figures and wrote the manuscript. Babett Steglich analyzed the Xenium data and supported sequencing data analyses. Alena Laschtowitz and Christian Casar performed bulk sequencing alignment. Hanna Ulrich and Ning Song supported the sequencing data analyses. Gerhard Schön and Antonia Zapf supported statistical analyses. Christina Weiler-Normann, Christoph Schramm and Ansgar Wilhelm Lohse designed and initiated the clinical trial and recruited patients. Malte Wehmeyer recruited patients and assisted in conducting the clinical trial. Ida Schregel provided the matched clinical registry data. Ludwig J. Horst, Silja Steinmann, Johannes Hartl, Marcial Sebode, Adrian Sagebiel and Jonas Wagner recruited participating patients. Michael Dudek and Jonas Fackler performed in vitro cytotoxic assays. Joseph Tintelnot performed single-cell sequencing. Laura A. Liebig performed single-nucleus sequencing. Varshi Sivayoganathan and Christian F. Krebs performed and supervised the Xenium spatial in situ RNA expression assay. Sören Alexander Weidemann and Jenny Krause collected and provided formalin-fixed paraffin-embedded tissue for analyses. Manuela Kolster performed pSTAT5 detection and supported T-cell *ex vivo* expansion experiments. Jing Lu provided additional support for *ex vivo* expansion experiments. Guido Rattay performed cytokine characterization in the T-cell activation experiments. Mariana V. Rosemblatt, Sarah Nuñez, Justine Castañeda, Maria Rosa Bono, Nico Kaiser, Maria Schwerk, Victor Puelles, Stefan Bonn, Marius Böttcher, Norbert Hübner, Eva Tolosa, Samuel Huber, and Percy A. Knolle provided critical intellectual input for experimental design and manuscript preparation. Johannes Herkel, Lorenz Adlung, Christoph Schramm, Nicola Gagliani and Ansgar Wilhelm Lohse provided critical intellectual input for the experimental design, conceived and designed experiments, acquired funding, supervised the study and wrote the manuscript. All co-authors critically revised the manuscript.

Data and code availability

The processed Seurat objects will be available on the Research Data Repository of the University of Hamburg (https://www.fdr.uni-hamburg.de/under the DOI 10.25592/uhhfdm.18135). Individual-level transcriptomic data and code are available upon reasonable request to the corresponding author.

Declaration of generative AI and AI-assisted technologies in the writing process

During the writing of the manuscript, the authors used openAI GPT4/4o to proofread some of the sentences.

Acknowledgements

We thank Madeleine Hamely for performing the final proofreading of the text.

Supplementary data

Supplementary data to this article can be found online at https://doi.org/10.1016/j.jhep.2026.02.026.

References

Author names in bold designate shared co-first authorship

[1] Slooter CD, van den Brand FF, Lleo A, et al. Lack of complete biochemical response in autoimmune hepatitis leads to adverse outcome: first report of the IAIHG retrospective registry. Hepatology 2024;79:538–550.

[2] Grønbæk L, Vilstrup H, Jepsen P. Autoimmune hepatitis in Denmark: incidence, prevalence, prognosis, and causes of death. A nationwide registry-based cohort study. J Hepatol 2014;60:612–617.

[3] European Association for the Study of the Liver. EASL Clinical Practice Guidelines on the management of autoimmune hepatitis. J Hepatol 2025;83:453–501.

[4] van den Brand FF, van der Veen KS, Lissenberg-Witte BI, et al. Adverse events related to low dose corticosteroids in autoimmune hepatitis. Aliment Pharmacol Ther 2019;50:1120–1126.

[5] Schmidt C, Stürznickel J, Strahl A, et al. Bone microarchitecture in patients with autoimmune hepatitis. J Bone Miner Res 2021;36:1316–1325.

[6] Lloyd C, Leighton J, Wong LL, et al. Patient priorities in autoimmune hepatitis: the need for better treatments, more education and challenging stigma. Dig Dis Sci 2023;68:87–97.

[7] Schramm C, Wahl I, Weiler-Normann C, et al. Health-related quality of life, depression, and anxiety in patients with autoimmune hepatitis. J Hepatol 2014;60:618–624.

[8] **Schmidt T**, **Schmidt C**, Strahl A, et al. A system to determine risk of osteoporosis in patients with autoimmune hepatitis. Clin Gastroenterol Hepatol 2020;18:226–233.e3.

[9] Schregel I, Papp M, Sipeki N, et al. Unmet needs in autoimmune hepatitis: results of the prospective multicentre European Reference Network Registry (R-LIVER). Liver Int 2024;44:2687–2699.

[10] Heneghan MA, Lohse AW. Update in clinical science: autoimmune hepatitis. J Hepatol 2025;82:926–937.

[11] **Zhang J**, **Guo L**, **Liu M**, et al. Receptor-interacting protein kinase 3 mediates macrophage/monocyte activation in autoimmune hepatitis and regulates interleukin-6 production. United Eur Gastroenterol J 2018;6:719–728.

[12] Tsikrikoni A, Kyriakou DS, Rigopoulou EI, et al. Markers of cell activation and apoptosis in bone marrow mononuclear cells of patients with autoimmune hepatitis type 1 and primary biliary cirrhosis. J Hepatol 2005;42:393–399.

[13] Zachou K, Rigopoulou EI, Tsikrikoni A, et al. Autoimmune hepatitis type 1 and primary biliary cirrhosis have distinct bone marrow cytokine production. J Autoimmun 2005;25:283–288.

[14] **de Boer YS**, **van Gerven NM**, Zwiers A, et al. Genome-wide association study identifies variants associated with autoimmune hepatitis type 1. Gastroenterology 2014;147:443. 52.e5.

[15] Kramer M, Mele F, Jovic S, et al. Clonal analysis of SepSecS-specific B and T cells in autoimmune hepatitis. J Clin Invest 2025;135:e183776.

[16] **Cardon A**, **Guinebretière T**, Dong C, et al. Single cell profiling of circulating autoreactive CD4 T cells from patients with autoimmune liver diseases suggests tissue imprinting. Nat Commun 2025;16:1161.

[17] Renand A, Cervera-Marzal I, Gil L, et al. Integrative molecular profiling of autoreactive CD4 T cells in autoimmune hepatitis. J Hepatol 2020;73:1379–1390.

[18] Wiggins BG, Pallett LJ, Li X, et al. The human liver microenvironment shapes the homing and function of CD4+ T-cell populations. Gut 2022;71:1399–1411.

[19] **Bovensiepen CS**, **Schakat M**, Sebode M, et al. TNF-producing Th1 cells are selectively expanded in liver infiltrates of patients with autoimmune hepatitis. J Immunol 2019;203:3148–3156.

[20] You Z, Li Y, Wang Q, et al. The clinical significance of hepatic CD69+ CD103+ CD8+ resident-memory T cells in autoimmune hepatitis. Hepatology 2021;74:847–863.

[21] Dudek M, Pfister D, Donakonda S, et al. Auto-aggressive CXCR6+ CD8 T cells cause liver immune pathology in NASH. Nature 2021;592:444–449.

[22] Laschtowitz A, Lindberg EL, Liebhoff AM, et al. Liver transcriptome analysis reveals PSC-attributed gene set associated with fibrosis progression. JHEP Rep 2024;7:101267.

[23] Hennes EM, Zeniya M, Czaja AJ, et al. Simplified criteria for the diagnosis of autoimmune hepatitis. Hepatology 2008;48:169–176.

[24] Brucklacher-Waldert V, Steinbach K, Lioznov M, et al. Phenotypical characterization of human Th17 cells unambiguously identified by surface IL-17A expression. J Immunol 2009;183:5494–5501.

[25] Müller-Dott S, Tsirvouli E, Vazquez M, et al. Expanding the coverage of regulons from high-confidence prior knowledge for accurate estimation of transcription factor activities. Nucleic Acids Res 2023;51:10934–10949.

[26] Aizarani N, Saviano A, Sagar, et al. A human liver cell atlas reveals heterogeneity and epithelial progenitors. Nature 2019;572:199–204.

[27] Andrews TS, Nakib D, Perciani CT, et al. Single-cell, single-nucleus, and spatial transcriptomics characterization of the immunological landscape in the healthy and PSC human liver. J Hepatol 2024;80:730–743.

[28] Segal JM, Kent D, Wesche DJ, et al. Single cell analysis of human foetal liver captures the transcriptional profile of hepatobiliary hybrid progenitors. Nat Commun 2019;10:3350.

[29] Kumar BV, Ma W, Miron M, et al. Human tissue-resident memory T cells are defined by core transcriptional and functional signatures in lymphoid and mucosal sites. Cell Rep 2017;20:2921–2934.
[30] Cheuk S, Schlums H, Gallais Sérézal I, et al. CD49a expression defines tissue-resident CD8+ T cells poised for cytotoxic function in human skin. Immunity 2017;46:287–300.
[31] Brockmann L, Soukou S, Steglich B, et al. Molecular and functional heterogeneity of IL-10-producing CD4+ T cells. Nat Commun 2018;9:5457.
[32] Baessler A, Vignali DAA. T cell exhaustion. Annu Rev Immunol 2024;42:179–206.
[33] Jin S, Plikus MV, Nie Q. CellChat for systematic analysis of cell-cell communication from single-cell transcriptomics. Nat Protoc 2025;20:180–219.
[34] Cepero-Donates Y, Rakotoarivelo V, Mayhue M, et al. Homeostasis of IL-15 dependent lymphocyte subsets in the liver. Cytokine 2016;82:95–101.
[35] Kim H, Hwang JS, Woo CH, et al. TNF-alpha-induced up-regulation of intercellular adhesion molecule-1 is regulated by a Rac-ROS-dependent cascade in human airway epithelial cells. Exp Mol Med 2008;40:167–175.
[36] Hartl J, Ehlken H, Sebode M, et al. Usefulness of biochemical remission and transient elastography in monitoring disease course in autoimmune hepatitis. J Hepatol 2018;68:754–763.
[37] Schultheiß C, Steinmann S, Willscher E, et al. Immune signatures in variant syndromes of primary biliary cholangitis and autoimmune hepatitis. Hepatol Commun 2023;7:e0123.
[38] Chaouali M, Ben Azaiez M, Tezeghdenti A, et al. High levels of proinflammatory cytokines IL-6, IL-8, TNF-A, IL-23, and IFN- in Tunisian patients with type 1 autoimmune hepatitis. Eur Cytokine Netw 2020 Dec;3. https://doi.org/10.1684/ecn.2020.0450.
[39] MacParland SA, Liu JC, Ma XZ, et al. Single cell RNA sequencing of human liver reveals distinct intrahepatic macrophage populations. Nat Commun 2018;9:4383.
[40] **Jin C**, **Jiang P**, **Zhang Z**, et al. Single-cell RNA sequencing reveals the pro-inflammatory roles of liver-resident Th1-like cells in primary biliary cholangitis. Nat Commun 2024;15:8690.
[41] **Mix H**, **Weiler-Normann C**, Thimme R, et al. Identification of CD4 T-cell epitopes in soluble liver antigen/liver pancreas autoantigen in autoimmune hepatitis. Gastroenterology 2008;135:2107–2118.
[42] Bielekova B, Muraro PA, Golestaneh L, et al. Preferential expansion of autoreactive T lymphocytes from the memory T-cell pool by IL-7. J Neuroimmunol 1999;100:115–123.
[43] Liu K, Catalfamo M, Li Y, et al. IL-15 mimics T cell receptor crosslinking in the induction of cellular proliferation, gene expression, and cytotoxicity in CD8+ memory T cells. Proc Natl Acad Sci U S A 2002;99:6192–6197.
[44] Alves NL, Hooibrink B, Arosa FA, et al. IL-15 induces antigen-independent expansion and differentiation of human naive CD8+ T cells in vitro. Blood 2003;102:2541–2546.
[45] Kim SH, Han SY, Azam T, et al. Interleukin-32: a cytokine and inducer of TNFalpha. Immunity 2005;22:131–142.
[46] Tiegs G, Horst AK. TNF in the liver: targeting a central player in inflammation. Semin Immunopathol 2022;44:445–459.
[47] Lampl S, Janas MK, Donakonda S, et al. Reduced mitochondrial resilience enables non-canonical induction of apoptosis after TNF receptor signaling in virus-infected hepatocytes. J Hepatol 2020;73:1347–1359.
[48] Plagiannakos CG, Hirschfield GM, Lytvyak E, et al. Treatment response and clinical event-free survival in autoimmune hepatitis: a Canadian multicentre cohort study. J Hepatol 2024;81:227–237.
[49] Björnsson HK, Gudbjornsson B, Björnsson ES. Infliximab-induced liver injury: clinical phenotypes, autoimmunity and the role of corticosteroid treatment. J Hepatol 2022;76:86–92.
[50] Weiler-Normann C, Schramm C, Quaas A, et al. Infliximab as a rescue treatment in difficult-to-treat autoimmune hepatitis. J Hepatol 2013;58:529–534.
[51] Efe C, Lytvyak E, Eşkazan T, et al. Efficacy and safety of infliximab in patients with autoimmune hepatitis. Hepatology 2025;81:1660–1670.
[52] Lewis JD, Scott FI, Brensinger CM, et al. Increased mortality rates with prolonged corticosteroid therapy when compared with antitumor necrosis factor-α-directed therapy for inflammatory bowel disease. Am J Gastroenterol 2018;113:405–417.
[53] Scott FI, Johnson FR, Bewtra M, et al. Improved quality of life with anti-TNF therapy compared with continued corticosteroid utilization in crohn's disease. Inflamm Bowel Dis 2019;25:925–936.
[54] Díaz-González Á, Schregel I, Carballo L, et al. Isolated IgG elevation in patients with persistently normal transaminases does not affect the outcome of autoimmune hepatitis. JHEP Rep 2025;7:101562.

Keywords: Autoimmune hepatitis; Infliximab; Tissue resident memory T cells; Auto-aggressive CD8$^+$ T cells; TNF; Immune cell network; Single-cell sequencing atlas.
Received 13 May 2025; received in revised form 13 February 2026; accepted 26 February 2026; available online 19 March 2026